The Astrophysical Journal, 633:122–137, 2005 November 1

MEASUREMENT OF GALAXY CLUSTER SIZES, RADIAL PROFILES, AND LUMINOSITY FUNCTIONS FROM SDSS PHOTOMETRIC DATA

Sarah M. Hansen,[1,2] Timothy A. McKay,[3] Risa H. Wechsler,[1,2,4] James Annis,[5]
Erin Scott Sheldon,[2] and Amy Kimball[6]

Received 2004 October 20; accepted 2005 July 3

ABSTRACT

Imaging data from the Sloan Digital Sky Survey are used to measure the empirical size-richness relation for a large sample of galaxy clusters. Using population subtraction methods, we determine the radius at which the cluster galaxy number density is $200\Omega_m^{-1}$ times the mean galaxy density, without assuming a model for the radial distribution of galaxies in clusters. If these galaxies are unbiased on megaparsec scales, this galaxy density–based R_{200} reflects the characteristic radii of clusters. We measure the scaling of this characteristic radius with richness over an order of magnitude in cluster richness, from rich clusters to poor groups. We use this information to examine the radial profiles of galaxies in clusters as a function of cluster richness, finding that the concentration of the galaxy distribution decreases with richness and is systematically lower than the concentrations measured for dark matter profiles in *N*-body simulations. Using these scaled radii, we investigate the behavior of the cluster luminosity function and find that it is well matched by a Schechter function for galaxies brighter than $M_r = -18$ only after the central galaxy has been removed. We find that the luminosity function varies with richness and with distance from the cluster center, underscoring the importance of using an aperture that scales with cluster mass to compare physically equivalent regions of these different systems. We note that the lowest richness systems in our catalog have properties consistent with those expected of the earliest forming halos; our cluster-finding algorithm, in addition to reliably finding clusters, may be efficient at finding fossil groups.

Subject headings: cosmology: observations — galaxies: clusters: general

Online material: color figures

1. INTRODUCTION

Galaxy groups and clusters appear in many guises. Observationally, they can be identified as pools of X-ray–emitting gas, collections of galaxies, Sunyaev-Zel'dovich decrements of the cosmic microwave background (CMB), or strong features in the gravitational shear field. Theoretically, they are identified as the largest overdense "halos" of dark matter. Mass is the key defining attribute of a galaxy cluster. The evolution of the cluster mass function and its variance plays an important role in constraining cosmological parameters describing dark energy, such as w and Ω_Λ (e.g., Lima & Hu 2005), and large-scale structure, such as Ω_m and σ_8 (e.g., Bahcall et al. 2003a). Mass estimates and studies of cluster members both rely on knowing the size of a cluster of given mass. To define the mass of a cluster, typically a cluster radius is specified through some prescription and the total mass taken to be the mass contained within that radius. Various operational definitions are used to determine cluster size and mass, but all of these show a regular increase in cluster size with mass. In order to study objects in a wide range of masses in a meaningful way, we must be able to determine an appropriate size scale for these clusters and groups; we may then use this characteristic scale as an aperture within which to make comparisons.

In numerical simulations, the precision of cluster mass and size measurements is limited only by resolution. Still, there are a variety of definitions for both size and mass in use, as discussed in some detail by White (2001). One class of estimates is based on top-hat filtered spherical overdensities. In this model, clusters are expected to be virialized within regions where the enclosed mean mass density exceeds the critical density by a factor $\Delta \sim 200$ (Peebles 1993, p. 25; Peacock 1999, p. 15). The radius at which this overdensity is reached, $R_{\Delta=200}$, is used as the characteristic radius of the cluster. The total mass within this radius, $M_{\Delta=200}$, is used as the characteristic mass. A number of choices of Δ are in use in the literature, from an overdensity of 180 times the mean background (e.g., Jenkins et al. 2001; Kravtsov et al. 2004), 200 times the critical density, i.e., $200\Omega_M^{-1}$ times the mean background (e.g., Diaferio et al. 2001; Evrard et al. 2002; Kochanek et al. 2003), to the "virial mass" (Eke et al. 1996; Bullock et al. 2001). Alternative definitions identify halos by "friends-of-friends" (FOF) methods (Davis et al. 1985; Jenkins et al. 2001). In these methods, particles are associated with halos to which they are linked by sequences of neighboring particles. Masses for FOF halos are often given by the sum of member particle masses, but as the halos are not required to be spherical, halo size is less clearly defined.

Observationally, cluster mass and size are difficult to measure directly; typically some mass estimator is adopted as a proxy, and typically a mass model is assumed to calculate the virial size. With deep observations, lensing may be used to make detailed mass maps of rich clusters, but this is not yet a practical technique for a large sample of systems spanning a wide range of masses. With large, shallower surveys, the lensing signals from a set of lens systems can be stacked to determine a composite mass profile (Sheldon et al. 2001). However, the large number of lens systems needed for high signal-to-noise ratio makes such a measurement

[1] Department of Astronomy and Astrophysics, University of Chicago, 5640 South Ellis Avenue, Chicago, IL 60637.
[2] Kavli Institute for Cosmological Physics, University of Chicago, 933 East 56th Street, Chicago, IL 60637.
[3] Physics Department, University of Michigan, 2477 Randall Laboratory, 500 East University Avenue, Ann Arbor, MI 48109.
[4] Hubble Fellow.
[5] Fermi National Accelerator Laboratory, P.O. Box 500, 500 Wilson Road, Batavia, IL 60510.
[6] Astronomy Department, University of Washington, Stevens Way, Box 351580, Seattle, WA 98195.

difficult for examining narrow mass ranges. While examining the lensing signal from an individual cluster recovers a specific mass, that estimate is affected by the errors, such as those due to projection effects, in modeling the mass. Combining the lensing signal from many clusters is advantageous because projection effects are unimportant, and the stacking simplifies modeling of neighboring structures. While stacking does limit the resolution in mass for a large set of clusters, this limitation is due to the amount of data available rather than the technique used. Other observational techniques for estimating mass, whether using X-ray temperature, SZ flux, or velocity dispersion as a mass estimator, also rely on either expensive spectroscopy to gain a detailed understanding of a few rich systems or models for the mass distribution used to infer the total system mass and size. To compare observational data to theoretical models and to compare the observed properties of clusters of different masses, it would be preferable to avoid using a model-dependent mass/radius scaling.

With a large photometric optical survey it is now possible to use cluster richness to characterize galaxy systems without suffering from the projection effects that have plagued such a mass estimator in the past. Since the cluster catalog of Abell (1958), systems of galaxies have been sorted and compared using a variety of richness parameters, many of which have been based on the number of galaxies within a certain luminosity range and distance from the estimated cluster center. The richness parameters of Abell et al. (1989), Couch et al. (1991), Dalton et al. (1992), Lumsden et al. (1992), Lidman & Peterson (1996), Postman et al. (1996), Ostrander et al. (1998), Olsen et al. (1999), Gladders (2002), Goto et al. (2002a), Postman et al. (2002), and Gal et al. (2003) are of this type; see Bahcall (1981), Yee & López-Cruz (1999), and Bahcall et al. (2003b) for further discussion and comparison of some of these richness estimators. We can stack systems in narrow richness bins and measure directly the distribution of galaxies in clusters over a wide range of masses. This galaxy distribution is used to estimate the virial size of these systems. Ideally, cluster members would be identified spectroscopically. Such data are not feasible to obtain for a very large sample of clusters, so we rely on projected photometric data taken in multiple bandpasses and correct for the foreground and background galaxies that contaminate our line of sight to each cluster.

The Sloan Digital Sky Survey (SDSS; York et al. 2000; Stoughton et al. 2002) data offer thousands of clusters and groups for study and can be used to measure excellent photometric redshifts for those objects. We use data from the SDSS to directly determine a size-richness relation for groups and clusters with a model-independent method. Since we cannot directly measure the radius at which the cluster has a mass overdensity of ΔM, we instead determine the radius $R_{\Delta}^{\mathcal{N}}$ at which the space density of cluster galaxies, $\mathcal{N}$, is overdense by $\Delta\mathcal{N}$. We present the scaling of $R_{200}^{\mathcal{N}}$ with richness, which can be employed to further study galaxy clusters and their members. For example, to study the relationship between different mass estimators, such as the mass from lensing measurements and the total luminosity of the cluster, it is essential to know this scaling of cluster size with richness.

If the distribution of galaxies in a halo traces the overall dark matter distribution, our galaxy density–based $R_{200}^{\mathcal{N}}$ will reflect the characteristic radius of clusters. In detail, the relation between the dark matter density profile and the radial distribution of a population of galaxies depends on a number of physical processes, including dynamical friction and tidal striping, and depends on the properties of the galaxy sample, but both simulations and previous observational work suggest that the distribution of galaxies in a halo at least roughly traces the overall dark matter distribution (e.g., Nagai & Kravtsov 2005; Lin et al. 2004).

This hypothesis is supported by recent lensing and galaxy clustering measurements (Sheldon et al. 2004; Weinberg et al. 2004), which suggest that the bias of typical SDSS galaxies is approximately 1 and is roughly scale independent on scales larger than a few hundred h^{-1} kpc. In any case, without assuming a model for the radial distribution of galaxies in clusters, we can directly measure the radius at which the galaxy density in clusters is Δ times more dense than the average background.

Our investigation does not distinguish between galaxy groups and clusters. Systems of galaxies come in a range of masses from single galaxies in larger halos up to the most massive of clusters. There is a clear boundary between galaxies and systems of galaxies; there is not any clear dividing point between poor and rich systems of galaxies as observed in the optical. We use the full range of our cluster finder to develop our catalog of systems; our mass estimator spans the range from highly populated clusters down to very sparse systems, and we refer to any system with two or more galaxies as a "cluster." There is no strong break in the properties of the systems found as a function of richness.

In § 2 we describe the SDSS data used and discuss the cluster-finding technique and richness measurement; in § 3 we present and test our method of background subtraction through examination of the radial profile and luminosity function (LF). Our calculation of $R_{200}^{\mathcal{N}}$ as a function of richness is presented in § 4. We further examine the radial density profile within $R_{200}^{\mathcal{N}}$ in § 5; we examine the LF within $R_{200}^{\mathcal{N}}$ and how the LF changes as a function of $r/R_{200}^{\mathcal{N}}$ for clusters of different richnesses in § 6. Throughout we assume a flat, ΛCDM cosmology with $H_0 = 100\,h$ km s^{-1} Mpc^{-1}, $h = 0.7$, and matter density $\Omega_m = 0.3$.

2. DATA

2.1. *SDSS Galaxies*

In this study we use 395 deg^2 of SDSS commissioning data (York et al. 2000), a subset of the Early Data Release data. In particular, we use the 170 contiguous square degrees imaged on 1998 September 19 and 25, covering the range $145\overset{\circ}{.}1 \leq$ R.A. $\leq 236\overset{\circ}{.}0$, $-1\overset{\circ}{.}25 \leq$ decl. $\leq +1\overset{\circ}{.}25$ (J2000.0), known as SDSS stripe 10, and the 225 contiguous square degrees imaged on 1999 March 20–21, covering the range $351^{\circ} \leq$ R.A. $\leq 56^{\circ}$, $-1\overset{\circ}{.}25 \leq$ decl. $\leq +1\overset{\circ}{.}25$ (J2000.0), known as stripe 82. Seeing varies on these two stripes from $1\overset{''}{.}0$ to $2\overset{''}{.}0$, and the data are photometrically uniform to within 3% (Hogg et al. 2001; Smith et al. 2002). Star-galaxy separation is robust to 21.0, 21.0, 21.0, and 19.8 in g, r, i, and z passbands, respectively (Scranton et al. 2002), which we adopt as the limiting apparent magnitudes for this work. All apparent magnitudes are measured by the photometric data processing pipeline using a modified version of the Petrosian (1976) system (for a discussion of the advantages of Petrosian magnitudes see Blanton et al. 2001) and are corrected for Galactic extinction using the dust maps of Schlegel et al. (1998). Further details about the photometric data and the parameters measured may be found in Lupton et al. (2001), R. H. Lupton et al. (2005, in preparation), and Stoughton et al. (2002).

2.2. *Cluster-finding Technique*

Clusters used in this study are detected by the maxBCG algorithm. This method relies on the observation that clusters host

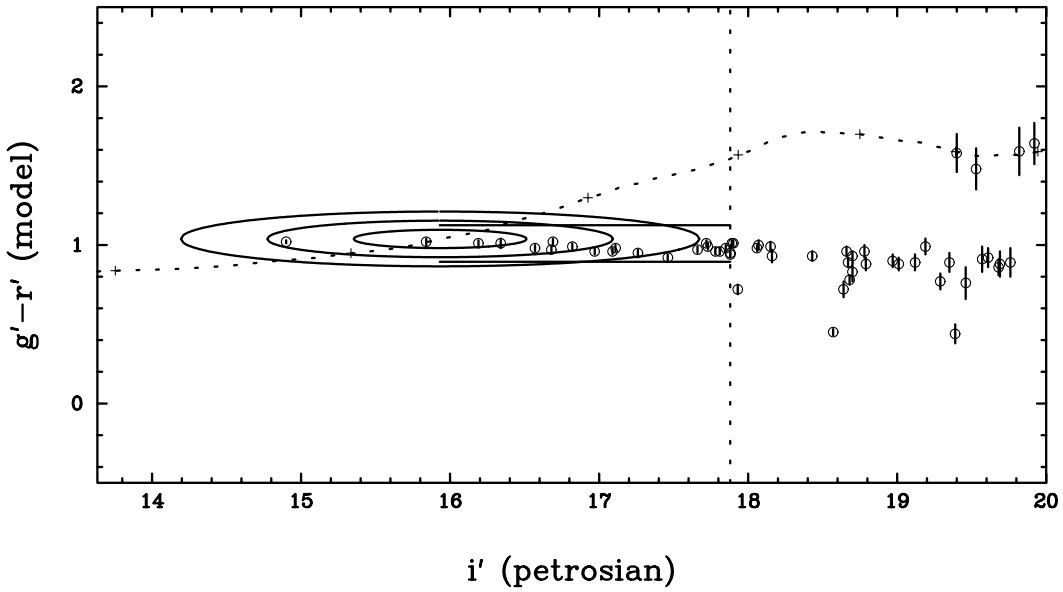

FIG. 1.—Color-magnitude diagram of observed $g - r$ vs. apparent i band for galaxies near a rich cluster at $z = 0.15$. Ellipses represent 1, 2, and 3 σ contours around the mean BCG color and magnitude at that redshift. The dotted line indicates the track of BCG color and magnitude as a function of redshift. The horizontal lines and vertical dashed line show the region of inclusion for $N_{\rm gal}$ determination. [*See the electronic edition of the Journal for a color version of this figure.*]

a population of early-type galaxies that have small dispersion in color (Bower et al. 1992; Stanford et al. 1995; Smail et al. 1998; Gladders & Yee 2000). These cluster members populate the red sequence on a color-magnitude diagram. The brightest cluster galaxies (BCGs) have colors that are compatible with the red sequence galaxies (Aragon-Salamanca et al. 1998; Nelson et al. 2002) and also have a very small dispersion in luminosity (Sandage 1972, 1976; Oemler 1976; Hoessel et al. 1980; Schneider et al. 1983; Postman & Lauer 1995; Collins & Mann 1998). There is evidence that the colors and magnitudes of BCGs remain predictable (and thus indicative of redshift) until at least $z = 0.6$ (Aragon-Salamanca et al. 1998; Nelson et al. 2002), shifting only due to passive evolution.

The maxBCG algorithm takes advantage of these observed properties to find BCGs and the galaxies that are associated with them. For every galaxy, the algorithm calculates the highest likelihood, $\mathcal{L}_{\rm max}$, that any given galaxy is a BCG (which means that the galaxy has the properties of a BCG plus has a red sequence around it) and then identifies clusters by finding galaxies with high $\mathcal{L}_{\rm max}$ values compared to the surroundings. $\mathcal{L}_{\rm max}$ for each galaxy is determined by finding the maximum of $\mathcal{L}(z)$, the calculated likelihood as a function of redshift for the candidate. The likelihood function $\mathcal{L}(z)$ is the sum of two terms and is calculated at every redshift from $z = 0.0$ to 0.6 in steps of 0.01. That is, for each galaxy we calculate

$$\mathcal{L}_{\rm max} = \max \mathcal{L}(z), \tag{1}$$

where $\mathcal{L}(z) = \mathcal{L}_{\rm BCG} + \log N_{\rm gal}$.

The first term, $\mathcal{L}_{\rm BCG}$, is the BCG likelihood: the likelihood that the galaxy in question is consistent with, compared to the known population dispersions, the apparent magnitudes and colors of the mean BCG population as seen at that redshift. These colors and magnitudes were derived from the properties of Abell clusters observed by the SDSS. The second term, $\log N_{\rm gal}$, is the log of the count of the other galaxies in the vicinity that are also of the right color and magnitude to be cluster members. To count the number of galaxies, we examine only those projected within 1 h^{-1} Mpc (at the redshift in question) that fall in the red sequence for each redshift. A galaxy is within the red sequence if it is within 2 σ ($\sigma = 0.05$ mag) of the mean BCG color at that redshift, fainter than the BCG candidate, and brighter than $M_i = -20.25$ (approximately $0.5L_*$). Figure 1 shows a color-magnitude diagram for a rich cluster. The region of inclusion for $N_{\rm gal}$ determination is shown by the contours; the color and apparent luminosity of a passively evolving BCG as a function of redshift are indicated by a dotted line. The interplay between finding a galaxy with the right color and luminosity to be a BCG and finding a galaxy with red sequence neighbors determines the redshift distribution of $\mathcal{L}(z)$. We find the redshift that maximizes $\mathcal{L}(z)$ for the galaxy in question. That galaxy is assigned $\mathcal{L}_{\rm max}$ and the corresponding redshift. At the end of this process each galaxy in the catalog has a single maximum likelihood and a single redshift.

We then need to select the cluster centers out of the catalog of all galaxies. We find the peaks in the distribution of $\mathcal{L}_{\rm max}$ over all galaxies; these peaks are the clusters. For each candidate BCG, we check whether its likelihood $\mathcal{L}_{\rm max}$ is the highest likelihood when compared with neighboring candidates within $\Delta z = 0.05$ that are projected within 1 h^{-1} Mpc of the BCG candidate in question. If the candidate BCG's $\mathcal{L}_{\rm max}$ is the greatest of those neighbors, we list the candidate in the cluster catalog as a BCG.

The cluster catalog produced contains information about each cluster identified, including the photometric properties of the BCG, the estimated redshift, and the richness, $N_{\rm gal}$. Each cluster center is taken to be at the location of its BCG. The richness measurement for the cluster, $N_{\rm gal}$, is defined to be the number of galaxies in the red sequence at the derived redshift. The resulting catalog contains objects over a wide range of richnesses: from quite poor systems of only a few galaxies ($N_{\rm gal} \leq 8$; $\sigma_v \leq 300$ km s^{-1}; 10,560 systems in $0.07 \leq z \leq 0.3$) to very massive clusters of hundreds of galaxies ($N_{\rm gal} \geq 30$; $\sigma_v \geq 700$ km s^{-1}; 19 systems in $0.07 \leq z \leq 0.3$). Figure 2 shows the distribution of identified objects as a function of redshift and richness. So as to avoid making an arbitrary distinction between a group and a cluster, we generically refer to a system

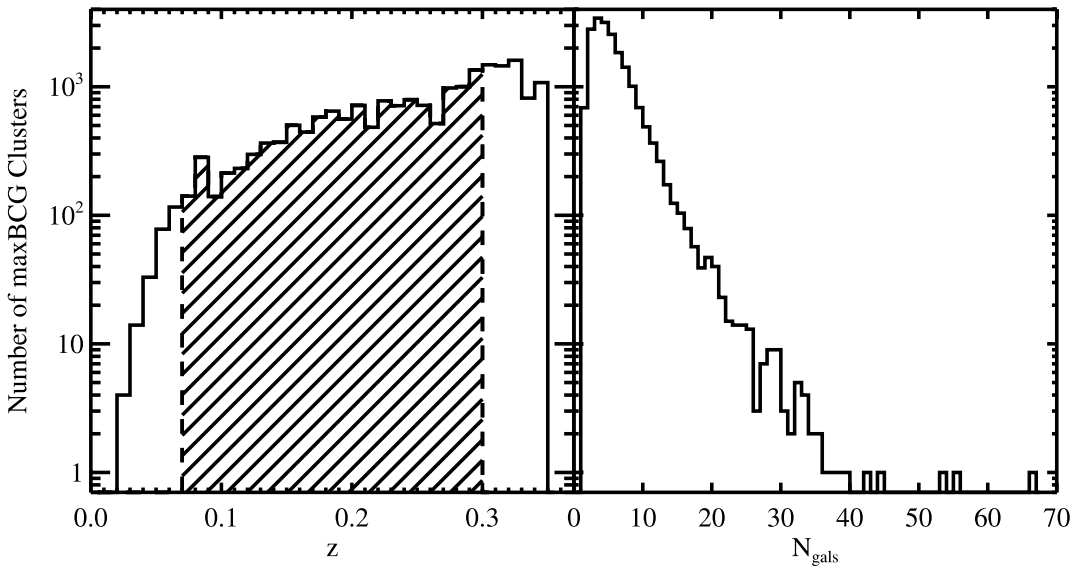

FIG. 2.—*Left*: Redshift distribution of maxBCG-identified objects. We use clusters in the shaded region; simulations show that the completeness rate begins to drop for $z > 0.3$. *Right*: Distribution of $0.07 \leq z \leq 0.3$ maxBCG-identified objects as a function of cluster richness, N_{gal}. There are 12,830 systems identified in this redshift range; 2270 of them have $N_{gal} \geq 8$, and 19 clusters have $N_{gal} \geq 30$.

of galaxies as a cluster and specify the value of N_{gal} of that system.

The maxBCG algorithm has been tested extensively for completeness and purity. All previously known Abell and NORAS X-ray clusters in the region surveyed are recovered. Simulations suggest that maxBCG recovers and correctly estimates the richness for greater than 90% of clusters and groups present with $N_{gal} \geq 15$ out to a redshift of $z = 0.3$. The completeness and selection function of the algorithm will be further explored in R. H. Wechsler et al. (2005, in preparation). The clusters identified by this algorithm have been compared with the objects found by different cluster-finding algorithms run on the same data set. Discussion of the differences between maxBCG and other algorithms can be found in Bahcall et al. (2003b).

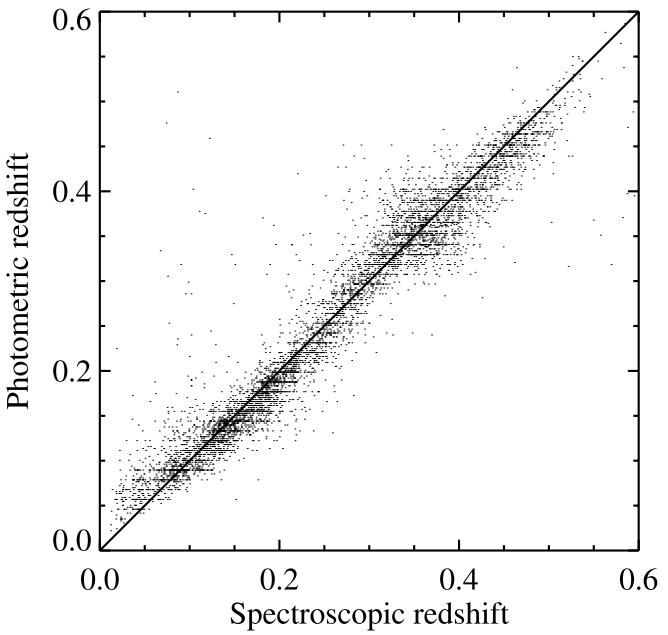

FIG. 3.—Photometric redshift estimation for the maxBCG cluster-finding algorithm tested here by comparison to spectroscopic redshift determination for a total of 6708 maxBCG clusters. The typical photo-z error is $\sigma_z = 0.02$ for the full sample, falling to $\sigma_z = 0.014$ for the redshift range $0.07 \leq z \leq 0.3$. The increase in photo-z errors around $z = 0.37$ occurs because this is where the 4000 Å break, the most significant feature in a typical galaxy spectrum, passes from the g to r filters. The clusters used in the comparison span the full range of N_{gal} of the catalog.

One of the strengths of this algorithm is that it is a robust photometric redshift estimator for the clusters: for the 6708 clusters in the catalog with spectroscopic redshifts available, the dispersion between the maxBCG estimated redshift and the spectroscopic redshifts is $\Delta z = 0.018$, as seen in Figure 3, and is smaller for the highest richness clusters. These 6708 systems span the range of N_{gal} in the catalog. As we do not have spectroscopic redshifts for all clusters examined but are confident in relying on these estimates, we henceforth use the term "redshift" to mean the estimated photometric redshift determined by maxBCG.

3. BACKGROUND SUBTRACTION

Given a set of cluster centers with well-defined three-dimensional positions, we need to find the galaxies associated with those clusters. This section explains how we apply background subtraction techniques to the SDSS data and how we check our method by constructing and examining the radial density profile and the LF.

Generically, any properties of galaxies in clusters can be described by some population distribution function (PDF) in a multidimensional parameter space. Properties of each galaxy such as luminosity, color, star formation rate, mass, and distance from the cluster center may be used as the parameters of a PDF. Examining how the galaxies of a particular cluster occupy the parameter space is a way to sample the PDF; with a large enough set of cluster galaxies, we may statistically determine the PDF quite well. The overall properties of the clusters (e.g., cluster mass or X-ray temperature) may be used to identify different sets of clusters, and the PDFs of galaxies in these different cluster samples may be compared. In this way, we can explore how the properties of galaxies in clusters are related to the characteristics of the host clusters.

Without redshifts for all galaxies, we can only examine the PDF of galaxies associated with clusters by making an appropriate

correction for the set of field galaxies projected by chance along the line of sight to the clusters. We assume that the presence of a cluster at some redshift does not affect field galaxies found along the same line of sight. That is, the PDF of galaxies projected around a cluster center has two independent components: the distribution of real cluster galaxies and the distribution of random background and foreground galaxies. To determine the projected, azimuthally averaged PDF of just the galaxies associated with clusters (the PDF_C), we examine the PDF of all galaxies projected around cluster centers (the PDF_{CF}) and the PDF of all galaxies projected around a set of random (field) points on the sky (the PDF_F). The PDF_C is determined by subtracting: $\mathrm{PDF}_C = \mathrm{PDF}_{CF} - \mathrm{PDF}_F$. Although we cannot identify exactly which galaxies make up a particular cluster, we can very accurately describe the mean properties of galaxies associated with a set of clusters.

There are a variety of ways in the literature for measuring the contribution of noncluster members without having spectroscopic information. Historically, the population of field galaxies was estimated from number-flux counts in separate surveys (e.g., Abell 1958; Lugger 1986; Colless 1989), although this method has the disadvantage of not having the cluster and field samples measured in the same set of data. More recently, some authors (Valotto et al. 1997; Paolillo et al. 2001; Goto et al. 2002b; Popesso et al. 2005) have measured the background in an annulus centered on the cluster, in order to ensure that the background measurement is made using data of similar depth and seeing as the data in the region of the cluster. Other authors, such as Andreon et al. (2004), estimated the background from a nearby control field or from the $\log N - \log S$ relationship from the same data set from which the cluster sample is drawn (Lin et al. 2004). Garilli et al. (1999) subtracted interlopers on the basis of color information, removing "galaxies with colors not matching the expected ones at the cluster redshift." As galaxy surveys increase in area, it becomes feasible to measure the background counts directly from the general field, as done by Gladders & Yee (2005). The SDSS data offer large regions of sky measured to the same depth and with the same seeing, so we are able to determine the contribution of field galaxies in the same data as the clusters without artificially restricting the field measurement to the cluster neighborhood or making assumptions about the color or luminosity distribution of cluster members. By using a set of random points as the locations around which the field galaxy population is determined, we measure the characteristics of all galaxies that are associated with clusters.

3.1. *Application to SDSS Data*

The SDSS is an ideal data set with which to examine the PDF of cluster galaxies because it provides sky coverage for a large number of clusters and ample blank sky for measuring the field distribution. The SDSS data offer a rich parameter space with which to define the PDF. Properties such as luminosity, color, star formation rate, and morphology may all be explored. In this work, for g, r, i, and z bands, we construct and examine the $\mathrm{PDF}_C(N_{\mathrm{gal}},\ r,\ M)$: the density function of cluster galaxies per surface area in a three-dimensional space of cluster richness N_{gal}, projected radius r, and absolute magnitude M. The PDF may then be projected onto the axis of absolute magnitude to show the LF of cluster members, or onto the axis of projected radius to show the radial density profile of the cluster. In this section we describe the samples of galaxies examined and, as the PDF_{CF} and PDF_F are constructed in the same manner, discuss the construction of a general $\mathrm{PDF}(N_{\mathrm{gal}},\ r,\ M)$.

3.1.1. *Cluster and Field Samples*

To measure the PDF_{CF}, we examine galaxies projected near the 12,830 maxBCG objects found in the redshift range $0.07 \leq z \leq 0.3$. These systems have richnesses in the range $2 \leq N_{\mathrm{gal}} \leq 66$. We use all galaxies projected within $2\ h^{-1}$ Mpc of the cluster centers and in the absolute magnitude range $-24 \leq M \leq -16$. We bin the data in $50\ h^{-1}$ kpc radial times $1N_{\mathrm{gal}}$ richness times 0.2 absolute magnitude bins. The number of galaxies in each bin is then normalized by the physical area observed in each bin. Details of the calculations are discussed below.

To determine the PDF_F, we examine galaxies along lines of sight to randomly chosen field locations. For each cluster, we choose five positions on the same $\sim 200\ \mathrm{deg}^2$ stripe of sky as the cluster, with random right ascension and declination. These field positions are assigned the same redshift as the cluster and labeled with the richness of that cluster. The resulting set of 64,150 field points are observed with the same seeing and to the same depth as the clusters, and for any set of clusters there is a set of field positions with the same redshift distribution. The same radial and magnitude ranges and bin widths used for the PDF_{CF} are applied to determine the PDF_F. All excess galaxies seen around cluster locations as compared to the field are identified as cluster galaxies.

3.1.2. *Absolute Magnitudes*

To calculate absolute magnitudes M, apparent magnitudes m must be corrected for luminosity distance, Galactic dust extinction, and K-corrections as

$$M = m - 5\log_{10}\left[\frac{D_L(z)}{10\ \mathrm{pc}}\right] - R - K(z), \qquad (2)$$

where $D_L(z)$ is the luminosity distance for our assumed cosmology; R is the correction for reddening, computed following Schlegel et al. (1998); and $K(z)$ is the appropriate K-correction.

K-corrections are necessary because galaxy magnitudes in the observed bandpasses correspond to different rest-frame magnitudes depending on the redshift of the galaxy. To compare magnitudes of galaxies at different redshifts, we apply a K-correction to convert all the magnitudes to a fixed set of bandpasses. To do so, we use the method of Blanton et al. (2003a; kcorrect v3_2) and, following Blanton et al. (2003b), K-correct all galaxies to $z = 0.1$. This redshift is chosen since it is close to the median redshift of the SDSS spectroscopic sample and thus requires the smallest typical corrections.

Although the true redshifts of the galaxies are unknown, we apply K-corrections and calculate luminosity distances as though all galaxies projected around a given point (cluster center or field location) are at the same redshift as that point. For the galaxies distributed at different redshifts along the line of sight, the resulting absolute magnitudes are not correct, but for galaxies actually located at the redshift of the given position (i.e., those galaxies physically associated with the cluster) the K-correction and $D_L(z)$ are appropriate. When the PDF_F is subtracted from the PDF_{CF}, the contribution from galaxies not at the redshift of the cluster is removed, leaving only the cluster galaxies for which D_L and $K(z)$ are correctly determined.

Our color-dependent K-corrections also affect the absolute magnitude to which the sample is complete and volume limited at a given redshift. Galaxies of different colors (therefore with different amounts of K-correction applied) and different apparent magnitudes can have the same absolute magnitude. Thus,

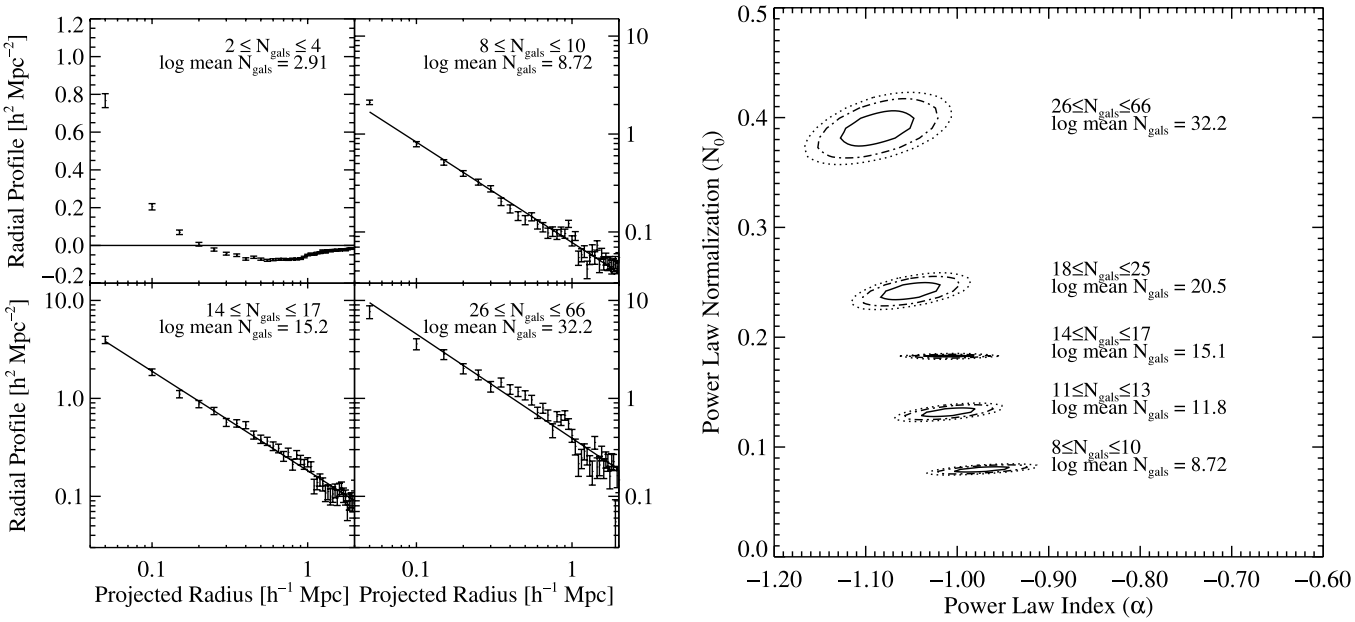

FIG. 4.—*Left*: Radial profiles of clusters for selected bins in richness. Shown are very poor (*upper left*), poor (*upper right*), medium (*lower left*), and high (*lower right*) richness clusters. The galaxies identified as BCGs have been removed. The lowest richness objects tend to be in underdense regions. For clusters with $N_{\rm gal} \geq 8$, a power law is a reasonable fit to the profiles. The best-fitting power law is shown. *Right*: Best-fit power-law parameters for the radial profiles of clusters of different richness. Shown are 1, 2, and 3 σ χ^2 contours of the model parameters for all richness bins with $N_{\rm gal} \geq 8$.

K-correcting a range of uncorrected absolute magnitudes $\delta M_{\rm uncorr}$ maps these magnitudes to the same $M_{\rm kcorr}$. For example, at $z = 0.3$, $\delta M_{\rm uncorr} \sim 0.4$ mag; at that redshift a galaxy with apparent r-band magnitude of 21.0 (the survey limit) corresponds, prior to K-correction, to an absolute magnitude of -19.9. To be complete to $z = 0.3$, we can only use those $M_{\rm kcorr}$ for which the corresponding range of $\delta M_{\rm uncorr}$ does not extend fainter than -19.9. The end result is that we adopt more conservative completeness limits to avoid color bias at faint luminosities. We do not use data in u band because both K-corrections and star-galaxy separation are not as robust in this passband. The resulting absolute magnitude limits for a complete (with volume limited to $z = 0.3$) sample of galaxies in g, r, i, and z are thus -20.2, -19.6, -19.4, and -20.6, respectively.

3.1.3. *Effects of Geometry and Luminosity*

We correct for incompleteness in both geometry and luminosity. Geometric incompleteness occurs when the search radius around clusters extends beyond the boundaries of the survey. For example, at a redshift of $z = 0.07$ (the lowest redshift cluster considered here), the 2 h^{-1} Mpc radius aperture is $\sim 0\overset{\circ}{.}75$ in diameter; some clusters lie too close to the edge of our $2\overset{\circ}{.}5$ wide stripe of sky to have all galaxies within the desired aperture contained on an observed region of sky. For each radial bin of each cluster, we account for this geometrical incompleteness by calculating the area that lies on an observed region and weight the galaxy counts in each bin accordingly.

Luminosity incompleteness arises because the apparent magnitude limit of the survey causes a varying range of absolute magnitudes to be accessible at varying redshifts. For example, to a redshift of 0.3, we can only see galaxies with $M_r < -19.6$ but can examine all clusters in our catalog, while at $z = 0.07$, we can see to $M_r \sim -16.5$ but are limited to only a few clusters. To avoid restricting ourselves to studying only galaxies brighter than the completeness limit of the full set of clusters (to $z = 0.3$), we account for this luminosity incompleteness. For each magnitude bin, we determine the number of clusters at redshifts low enough to have galaxies observable to that limit. The galaxy counts in each bin are weighted accordingly. The result is that the bright end of the luminosity distribution is based on galaxies in all clusters in the catalog (at redshifts out to $z = 0.3$), but the faint end is determined from galaxies associated with lower redshift clusters only. For our determination of $R_{200}^{\mathcal{N}}$, we use absolute magnitude limits that ensure luminosity completeness for the full set of clusters and push fainter only for examining the LF of cluster galaxies.

Having calculated the radial and absolute magnitude distributions of galaxies, we can determine the normalized PDF($N_{\rm gal}$, r, M) per surface area for galaxies around any set of positions and test our algorithm.

3.2. *Consistency Checks*

In this section we check the background subtraction technique by examining the radial distribution and the luminosity distribution of galaxies around field locations and compare these distributions to those measured around cluster centers.

Note that only a background-subtracted PDF (e.g., the PDF$_C$) contains physically meaningful information; the PDF around any set of points before subtraction is dominated by galaxies projected by chance along the same line of sight, which have not been properly K-corrected. We therefore reserve the name "luminosity function" for the projection of a background-subtracted PDF onto the axis of absolute magnitude; such a projection for a nonsubtracted PDF we refer to as a "luminosity distribution." Likewise, we reserve the term "radial profile" for background-subtracted PDFs only and refer to the "radial distribution" of galaxies when discussing a nonsubtracted PDF.

A check on the errors recovered by our background subtraction technique is done by comparing the PDF$_F$ with the population density of galaxies around a set of random points, which are different random points than those used in constructing the PDF$_F$. The PDFs measured around two different sets of random points should be statistically identical.

3.2.1. *Radial Number Density Profile*

A radial number density distribution is constructed by projecting a PDF($N_{\rm gal}$, r, M) onto the axis of projected radius. Examining the distribution of galaxies around field locations enables us to check our correction for incompleteness due to geometry.

When we construct the radial profile of clusters, we first examine the profile using only galaxies brighter than the completeness limit for the full set of clusters and then using all galaxies while accounting for the varying completeness limit as described above. The results are statistically the same but allow for inclusion of fainter galaxies in the latter case.

The radial distribution of galaxies around random points is flat, demonstrating that we are properly calculating the area observed when correcting for geometrical incompleteness. Comparing the radial distribution around field locations with that measured around a different set of random points, we see that the distributions are statistically identical at all radii. Any differences are within the error bars, which reflect the Poisson fluctuation of our sample.

Around cluster centers, however, we find a significant excess of galaxies compared to the field. This excess varies as a function of radius and as a function of richness. The left panel of Figure 4 shows the radial profile for selected richness bins corresponding to very low, low, medium, and high richness clusters, with the galaxies identified as BCGs removed. For clusters with $N_{\rm gal} \geq 5$, a power law is an acceptable fit to the profiles. For sets of clusters of different richness and $N_{\rm gal} \geq 8$, the radial profile is roughly consistent with a $\sim r^{-1.1}$ surface density profile, and thus an $r^{-2.1}$ volume density profile, but with increasing normalizations for richer clusters, reflecting the larger size of more massive clusters. For all richness bins above $N_{\rm gal} \geq 8$, the χ^2 contours of the power-law parameters are plotted as a function of cluster richness in the right panel of Figure 4. In § 5 we further examine the radial profiles, using our measurement of $R_{200}^{\mathcal{N}}$ to fit a Navarro et al. (1997) profile.

The lowest richness objects ($2 \leq N_{\rm gal} \leq 4$) tend to be in underdense regions. That is, compared to the distribution of galaxies around a random point in the universe, these systems of just a few red galaxies tend to have few nearby neighbors. We do not expect these very low $N_{\rm gal}$ objects to be representative of the full population of low-mass halos, as selection effects of the maxBCG algorithm are significant for these systems. Nonetheless, such a sample is interesting; we discuss very low $N_{\rm gal}$ systems in more detail in § 7.

3.2.2. *Luminosity Function*

The LF of galaxies in clusters is the projection of the PDF$_C$($N_{\rm gal}$, r, M) onto the absolute magnitude axis. The result is the mean number of galaxies per cluster per unit surface area as a function of luminosity and richness.

We check our background subtraction and incompleteness correction by comparing the luminosity distribution around two different sets of random points, expecting no significant difference. We begin by selecting only locations with low redshift, so that the luminosity distribution may be examined to faint magnitudes without weighting for the redshift distribution, and then also check the distribution with the full sample and appropriate weighting as discussed in § 3.1.3. The two samples have identical distributions.

The luminosity distribution contains a statistically significant excess of galaxies around cluster centers compared to galaxies around field locations. Figure 5 shows our determination of the LF of galaxies that are in rich clusters ($30 \leq N_{\rm gal} \leq 66$) and are within 1.5 h^{-1} Mpc of the cluster center, both before and after subtraction of the field (*top and bottom panels*, respectively).

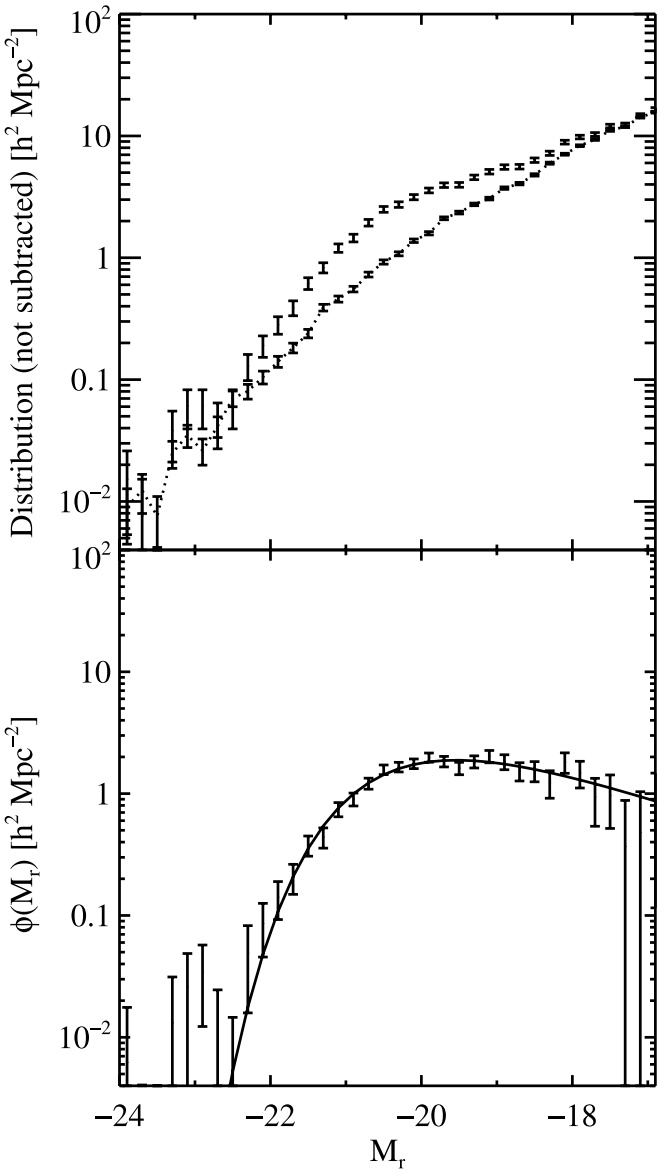

FIG. 5.—LF per unit surface area in r band for galaxies in rich clusters ($30 \leq N_{\rm gal} \leq 66$), using galaxies within a fixed 1.5 h^{-1} Mpc aperture. *Top* (*before subtraction*): Luminosity distribution of galaxies projected around cluster centers and field points (*dotted line*). Because we *K*-correct all galaxies to the cluster redshift regardless of the true redshift of each galaxy, the luminosity distribution around random points does not look like the LF of galaxies as measured by, e.g., Blanton et al. (2003b). *Bottom* (*after subtraction*): LF of galaxies associated with these rich clusters. The solid line is the best-fitting Schechter function.

In the bottom panel the solid line plots the best-fitting Schechter function (Schechter 1976), of the form

$$\phi(M)\,dM = 0.4\ln(10)\phi_* 10^{-0.4(M-M_*)(\alpha+1)} e^{-10^{-0.4(M-M_*)}}\,dM, \tag{3}$$

where α is the faint-end slope and M_* is the turnover magnitude; we fit the data using the Levenberg-Marquardt χ^2 minimization procedure. We recover an LF that is comparable to that of rich clusters found by Goto et al. (2002b), who used different cluster-finding and background subtraction algorithms with the same sample of SDSS data used in this paper.

We also examine the LF of cluster galaxies in three redshift slices to test whether our weighting scheme for the faint end is

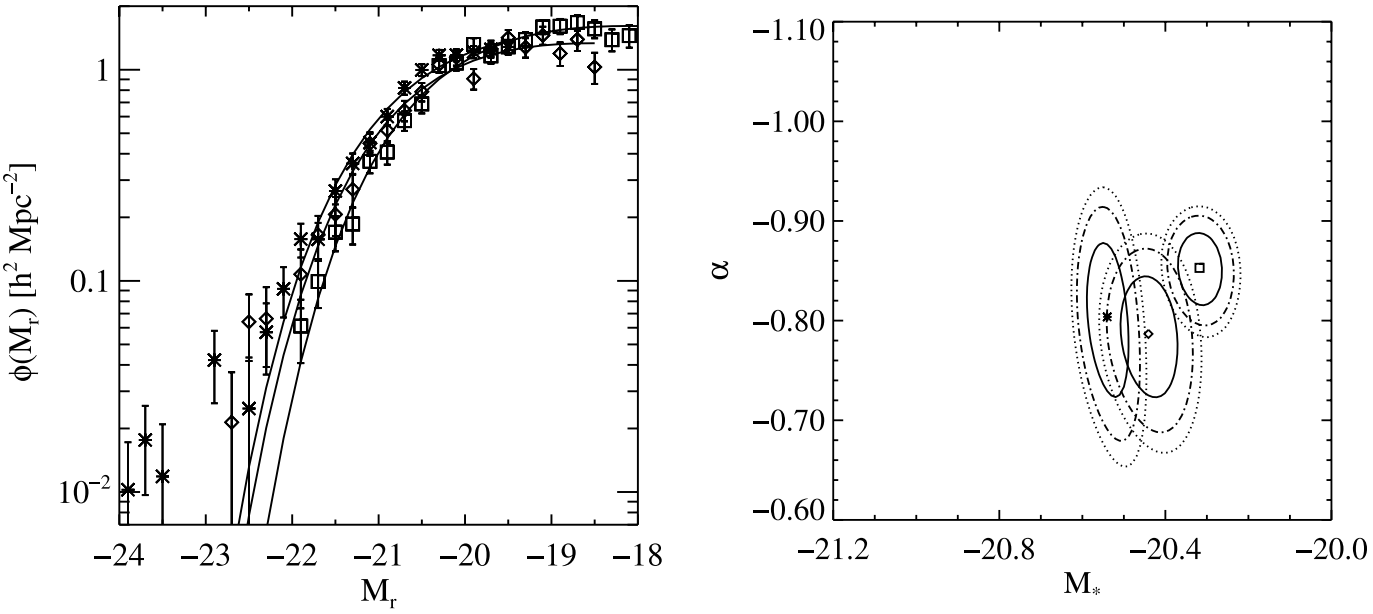

FIG. 6.—*Left*: LF per unit surface area in *r* band for clusters with $18 \leq N_{\rm gal} \leq 66$ in three redshift slices. Cluster members used are projected within 1.5 h^{-1} Mpc of the cluster center. The BCGs have been removed. Squares are for clusters in $0.07 \leq z \leq 0.15$; diamonds for $0.15 < z \leq 0.20$; stars for $0.20 < z \leq 0.30$. The best-fitting Schechter functions are overlaid. *Right*: The 1, 2, and 3 σ χ^2 contours of the Schechter function parameters. The shift in the characteristic luminosity, M_*, reflects the passive evolution of the early-type galaxies.

correct. The left panel of Figure 6 shows the LF for clusters with $18 \leq N_{\rm gal} \leq 66$ for $0.07 \leq z < 0.15$, $0.15 \leq z < 0.20$, and $0.20 \leq z < 0.30$. Galaxies projected within 1.5 h^{-1} Mpc are used; the BCGs are not included. We fit each distribution with a Schechter function (*solid lines*). The confidence ellipses for the fit parameters α and M_* are plotted in the right panel of the figure. The only difference we detect between the LFs in different *z* slices is at the bright end, as reflected by the shift of M_* toward fainter magnitudes at lower redshifts. This shift is comparable to what is expected due to passive evolution of the red sequence galaxies in the clusters. As our *K*-corrections are nonevolving, we expect M_* to be $\sim$0.25 mag brighter for the highest redshift bin than for the low-*z* bin due to passive evolution. We note that these LFs are measured within a fixed physical aperture for systems of a wide range of richnesses. We present this comparison of LFs for redshift slices only as a check that we are recovering sensible LFs. A more detailed investigation of the evolution of the LF of cluster galaxies will be done in later work.

Since more massive clusters are larger, measuring the LF (or any other projection of the PDF that varies radially) within a fixed physical aperture samples different parts of clusters of different richnesses. For example, as can be seen from the radial profiles in Figure 4, a 1 h^{-1} Mpc radius around a poor group encompasses the entirety of the group but only samples the inner region of a rich cluster. Thus, in order to compare the LF of cluster galaxies in clusters of different richness, we should examine the LF of only those galaxies within some aperture that scales with richness. In addition, the LF of cluster galaxies may vary with radius. To compare radial trends in clusters of different richness, we should also use an appropriately scaled aperture. In § 4 we present our calculation of a characteristic radius of clusters as a function of richness, and we return to a discussion of the dependence of the LF on richness and radius in § 6.

4. $R_{200}^{\mathcal{N}}$ DETERMINATION

To appropriately compare properties of low- and high-mass objects, we need to understand how the characteristic size of clusters varies with richness. Motivated by the way R_Δ is defined in *N*-body simulations, as the threshold radius interior to which the mean mass density of a cluster is Δ times the average mass density, we define an analogous $R_{200}^{\mathcal{N}}$ using the space density $\mathcal{N}$ of galaxies in clusters compared to the average space density of galaxies. If galaxies are unbiased with respect to dark matter on all scales, we would have $R_\Delta^{\mathcal{N}} = R_\Delta$. Since the bias is close to unity, we accept $R_\Delta^{\mathcal{N}}$ as a reasonable approximation. Following simulations, we use $\Delta = 200$ as our threshold mean overdensity of cluster galaxies, which occurs at the radius $R_{200}^{\mathcal{N}}$.

Some authors take the average mass density to be the critical density, while others use the actual mean background density. For the main result of this paper, the scaling of $R_{200}^{\mathcal{N}}$ with cluster richness, we present results both using an overdensity threshold of $\Delta\mathcal{N}_{\rm crit} \equiv 200$ times the critical density and using $\Delta\mathcal{N}_{\rm mean} \equiv 200$ times the mean background density. We find the same scaling using either threshold. We intend to compare this work with the results using the Hubble volume simulations of Evrard et al. (2002), who use an overdensity threshold measured with respect to the critical density. Therefore, for investigations regarding the cluster galaxy population within $R_{200}^{\mathcal{N}}$, we present results using $\Delta\mathcal{N}_{\rm crit}$. Throughout this work we use the term $R_{200}^{\mathcal{N}}$ to mean the radius interior to which the mean number density of galaxies is $200\Omega_m^{-1}$ times the mean space density of galaxies, or equivalently 200 times the critical density.

To determine the mean space density of field galaxies, we use the *g*, *r*, *i*, and *z* LFs of Blanton et al. (2003b), which are properly normalized to a volume density and are determined with an SDSS spectroscopic sample of galaxies from the same region of sky. We integrate these field LFs down to the absolute magnitude limits applied to our cluster sample (-20.2, -19.6, -19.4, and -20.6 in *g*, *r*, *i*, and *z*, respectively) and take the resulting value to be the average space density in that passband. We use only these four bands since the *u*-band *K*-corrections and star-galaxy separation are not as robust as in these bands.

To measure the mean space density of cluster members, we use the $\mathrm{PDF}_C(N_{\rm gal},\ r,\ M)$ determined above for each richness.

For clusters of a given richness and in a given bandpass, in each radial bin r we sum over all bins with radius $\leq r$ and with absolute magnitude brighter than the completeness limit. We assume that the galaxies are contained in a sphere of radius r to calculate the volume density, then divide by the mean space density of field galaxies to get the fractional excess. In actuality, the galaxies are contained in a cylinder of diameter $2r$. Thus, although the uncorrelated galaxies are removed from the measurement, there is an excess of galaxies at radius r due to the projection. This excess depends on the shape of the radial density profile. For samples that have the same radial profile, this excess is simply the same multiplicative factor for all. For example, if the profile is $1/r^2$, the factor is $\pi/2$.

We then use the binned mean overdensity versus radius information to find the radius interior to which the number density of cluster galaxies is $200\Omega_m^{-1}$ times greater than the field density. Since the density has roughly a power-law radial dependence, to determine exactly where $\Delta\mathcal{N} = 200\Omega_m^{-1}$, we fit a line in log-log space in the region in which the overdensity passes through $200\Omega_m^{-1}$. The errors on this fit include the uncertainty on the density value and the width of the radial bin and determine the uncertainty in the $R_{200}^{\mathcal{N}}$ value. In this manner we calculate $R_{200}^{\mathcal{N}}$ for each $N_{\rm gal}$ bin for which there is at least one cluster.

The relationship between characteristic radius $R_{200}^{\mathcal{N}}$ and cluster richness $N_{\rm gal}$ is well fitted by a power law with index $\sim$0.6. The determination of $R_{200}^{\mathcal{N}}$ for clusters as a function of richness is the principle result of this work. Figure 7 shows $R_{200}^{\mathcal{N}}$ measured with r-band data as a function of $N_{\rm gal}$ (*diamonds*), with the best-fit power law plotted. We also plot the relationship between radius and richness measured using $\Delta\mathcal{N}_{\rm mean}$. The scaling is the same, with different normalization. Similar results are obtained for g, i, and z; the best-fit power-law parameters with 1 σ uncertainties are listed in Table 1 for all four passbands and both overdensity thresholds.

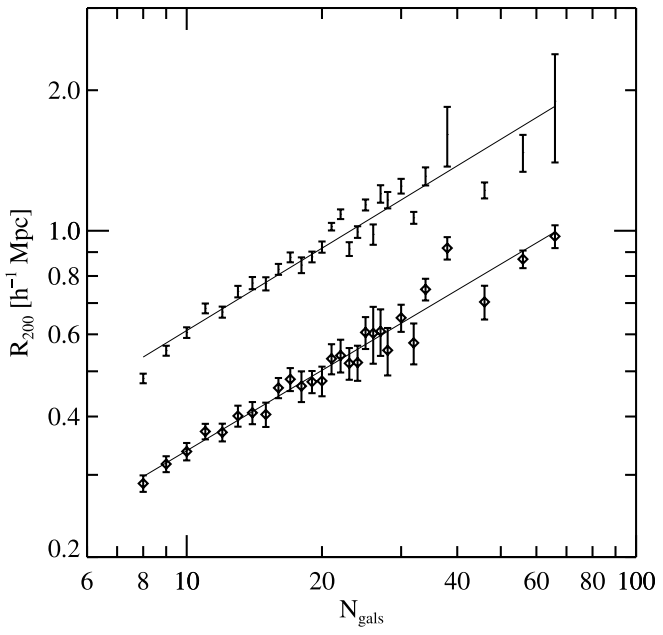

FIG. 7.—Relationship of the cluster characteristic radius, $R_{200}^{\mathcal{N}}$, here measured in r band, to richness, $N_{\rm gal}$. Diamonds mark the data using the overdensity threshold $\Delta\mathcal{N}_{\rm crit} \equiv 200$ times the critical density; the other data points use the overdensity threshold $\Delta\mathcal{N}_{\rm mean} \equiv 200$ times the mean density. Using either overdensity threshold results in a trend well fitted by a power law with the same scaling. Table 1 lists the best-fit values of the parameters.

TABLE 1
POWER-LAW FITS FOR $R_{200}^{\mathcal{N}}$ ($N_{\rm gal}$)

	$\Delta = 200$ CRITICAL		$\Delta = 200$ MEAN	
BAND	Index	Normalization	Index	Normalization
g.....	0.46 ± 0.03	0.17 ± 0.01	0.47 ± 0.03	0.28 ± 0.02
r.....	0.57 ± 0.02	0.091 ± 0.004	0.57 ± 0.01	0.159 ± 0.005
i.....	0.58 ± 0.02	0.083 ± 0.004	0.60 ± 0.01	0.142 ± 0.004
z.....	0.57 ± 0.02	0.097 ± 0.004	0.58 ± 0.01	0.172 ± 0.004

Under the assumption that the $R_{200}^{\mathcal{N}}$ we have measured here for clusters is a good proxy for a mass density–based R_{200} for dark matter halos, what sort of scaling relation would we expect with $N_{\rm gal}$? A detailed answer to this question requires understanding the mass-to-light ratio as a function of both cluster mass and cluster radius, which is beyond the scope of this paper. In the simple scaling arguments below, we assume that these are both constant. The radius and mass of a cluster scale as $R_{200} \sim M_{200}^{1/3}$, and the number of galaxies within R_{200} is likely to scale as a power law with cluster mass as $N_{{\rm gal},R_{200}} \sim M_{200}^{\alpha}$. This power has been found to be close to unity (e.g., Kravtsov et al. 2004; Lin et al. 2004; Zehavi et al. 2004; R. H. Wechsler et al. 2005, in preparation). The $N_{\rm gal}$ we use here, however, is measured within a fixed 1 h^{-1} Mpc radius aperture; it will typically be smaller than $N_{{\rm gal},R_{200}}$ for the most massive clusters and larger than $N_{{\rm gal},R_{200}}$ for smaller groups and clusters, roughly consistent with $N_{\rm gal} \sim N_{{\rm gal},R_{200}}^{\beta}$, with $\beta < 1$. If the galaxies follow an NFW profile out to $\max(1\ {\rm Mpc},\ R_{200})$, with a concentration around 5, one would expect β to be in the range $\sim$0.50–0.65. For maxBCG clusters that have been found in the simulations of R. H. Wechsler et al. (2005, in preparation), we find something similar: $N_{\rm gal} \sim N_{{\rm gal},R_{200}}^{0.56}$. Putting this all together, we have

$$R_{200} \sim M_{200}^{1/3} \sim N_{{\rm gal},R_{200}}^{1/(3\alpha)} \sim N_{\rm gal}^{1/(3\alpha\beta)} \sim N_{\rm gal}^{0.6}, \qquad (4)$$

which is in excellent agreement with the scaling relationship that we find for $R_{200}^{\mathcal{N}}$ and $N_{\rm gal}$. This comparison suggests that our observationally determined $R_{200}^{\mathcal{N}}$ is a reasonably good proxy for R_{200}. Note that in detail the relation between $N_{\rm gal}$ measured at a fixed radius and $N_{{\rm gal},R_{200}}$ is not expected to be a power law over all halo masses, which implies that the power-law relation found between R_{200} and $N_{\rm gal}$ may break down when measured over a wide range of halo mass. This relationship, as well as the detailed relationship between $R_{200}^{\mathcal{N}}$ and R_{200} as traced by dark matter, will be explored further in future work, using a larger sample and comparison to simulations.

5. GALAXY DENSITY PROFILES WITHIN $R_{200}^{\mathcal{N}}$

Using our empirically measured $R_{200}^{\mathcal{N}}$, we now examine the radial density profiles of galaxies in these clusters in greater detail. Simulations suggest that dark matter halos have mass profiles characterized by a scale radius $r_s \equiv R_{200}/c_{\rm DM}$, where $c_{\rm DM}$ is the concentration parameter for the dark matter (NFW; Navarro et al. 1997). Galaxies do not necessarily trace the same detailed distribution as the dark matter. In particular, for any given sample of galaxies chosen with some selection criteria, a range of processes (e.g., dynamical friction, tidal stripping, enhanced or suppressed star formation) may affect the distribution of those galaxies within their host dark matter halos. Still, several recent studies have suggested that the number density profile of galaxies is well described by the NFW function (e.g., Carlberg et al. 1997b; van der Marel et al. 2000; Mahdavi

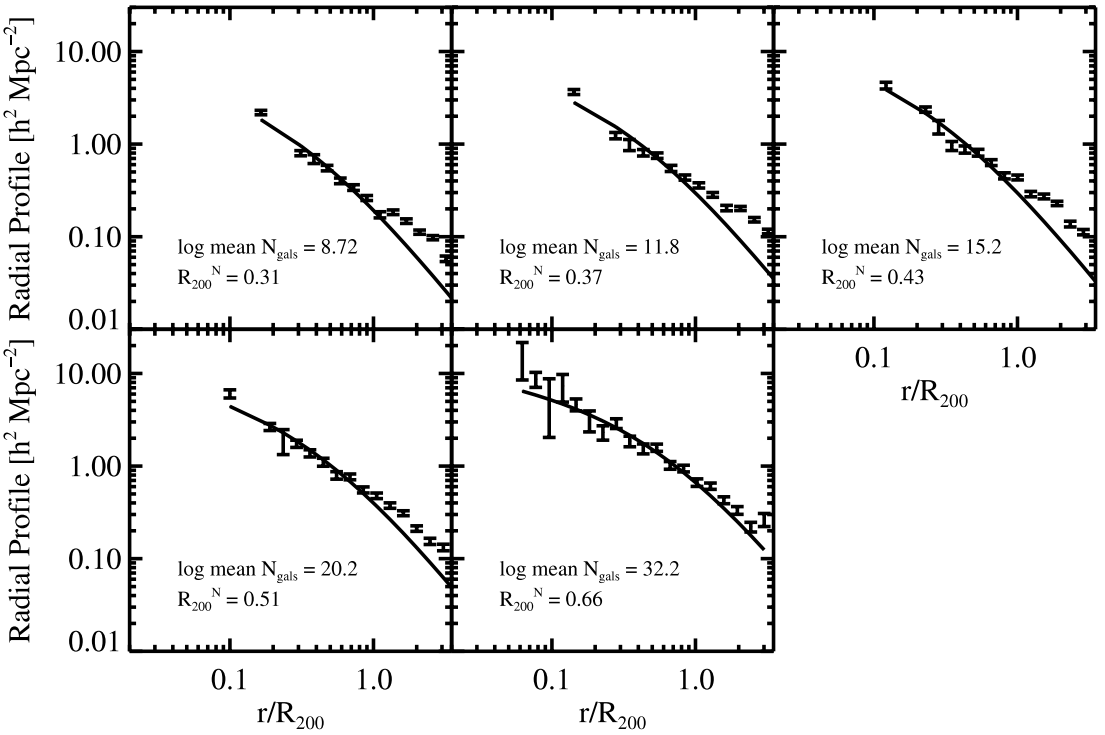

FIG. 8.—Number density profiles for satellite galaxies in clusters of different richness. The best-fit projected NFW profile is shown, obtained by assuming the previously measured relation between $R_{200}^{\mathcal{N}}$ and $N_{\rm gal}$ and fitting the data within $R_{200}^{\mathcal{N}}$ only. The $R_{200}^{\mathcal{N}}$ corresponding to the mean $\log N_{\rm gal}$ value of the richness bin is listed. The richness bins are the same used in examining the radial profiles previously (Fig. 4). The excess beyond $R_{200}^{\mathcal{N}}$ is to be expected as the two-halo term becomes important.

& Geller 2004; Katgert et al. 2004; Lin et al. 2004); here we fit our radial profiles with the projected NFW profile and examine its dependence on cluster richness.

We express the number density profile in three dimensions as $n(x) = n_0 x^{-1}(1+x)^{-2}$, with normalization n_0 and $x \equiv c_{\rm gal} r/R_{200}^{\mathcal{N}}$, where $c_{\rm gal}$ is the concentration parameter of the galaxies. Following Bartelmann (1996), we write the projected surface density NFW as the integral

$$\Sigma(x) = \frac{2n_0 R_{200}^{\mathcal{N}}}{c_{\rm gal}} \int_0^{\pi/2} \cos\theta \left(\cos\theta + \frac{c_{\rm gal} r}{R_{200}^{\mathcal{N}}}\right)^{-2} d\theta. \quad (5)$$

For several bins in richness, we express the radial profile in units of $r/R_{200}^{\mathcal{N}}$, where each cluster has been scaled by the $R_{200}^{\mathcal{N}}$ appropriate for its $N_{\rm gal}$ value, as measured in the previous section and specified in Table 1. We fit the resulting number density profile within $R_{200}^{\mathcal{N}}$ with the profile specified in equation (5); the results are shown in Figure 8. The fit does well for most of the richness bins. There is some excess outside the virial radii, which is to be expected as the two-halo term begins to contribute to the distribution. However, for the low-richness systems, some of this excess may be due to a misidentification of the cluster center. We discuss this issue further in § 6.

The variation of the concentration parameter with richness is shown in Figure 9. Note that we have defined the concentration parameter for galaxies with respect to the measured $R_{200}^{\mathcal{N}}$ of the galaxy profile; if this is not equivalent to the dark matter R_{200}, then $c_{\rm gal}$ will change accordingly. In the top panel of Figure 9 we show the measured $c_{\rm gal}$ divided by the expected dark matter concentration $c_{\rm DM}$, using the model of Bullock et al. (2001) assuming a cosmology with $\Omega_m = 0.3$. and $\sigma_8 = 0.9$. In order to make the comparison, we *assume* that $R_{200}^{\mathcal{N}} = R_{200}$, which may

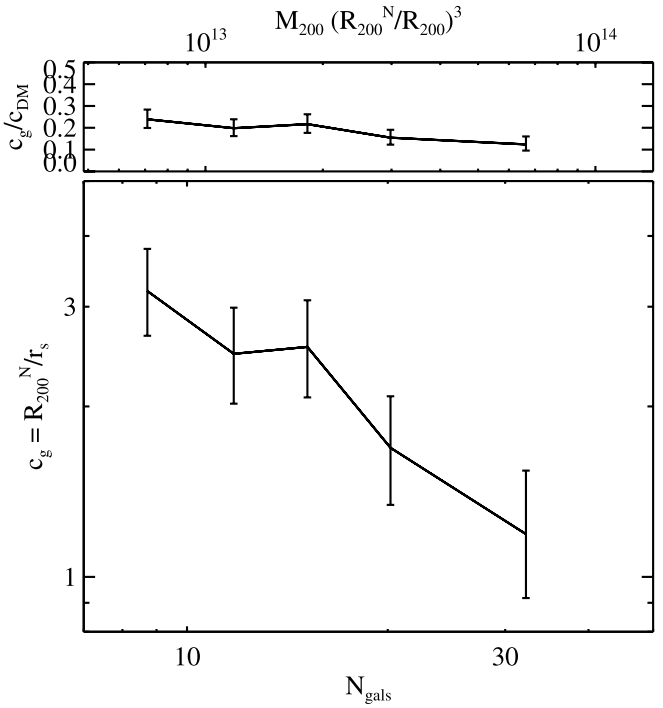

FIG. 9.—Best-fit concentration parameter of the galaxy profile, assuming that $R_{200}^{\mathcal{N}}$ is given by the previously determined relation between $R_{200}^{\mathcal{N}}$ and $N_{\rm gal}$. The error bars are determined from the 1 σ region of the χ^2 surface. The top axis shows M_{200}, assuming the same $R_{200}^{\mathcal{N}}$-to-$N_{\rm gal}$ scaling and under the assumption that $R_{200}^{\mathcal{N}} = R_{200}$ and $\Omega_m = 0.3$.

not be the case, especially for distributions with such different concentrations. In particular, preliminary indications from both simulations and weak-lensing measurements indicate that $R_{200}^{\mathcal{N}} < R_{200}$. Because the theoretical prediction for $c_{\rm DM}(M)$ gets steeper at higher masses, in this case $c_{\rm gal}(M)/c_{\rm DM}(M)$ would be closer to a constant with mass M.

It is clear that the profiles of galaxies in maxBCG clusters have significantly lower concentrations than the dark matter profiles measured in CDM N-body simulations. This finding is in agreement with previous work (e.g., Lin et al. 2004; Carlberg et al. 1997b; van der Marel et al. 2000), which has found $c_{\rm gal} \sim 2-4$ for cluster galaxies. These low values, however, should be interpreted as indications of how galaxies are distributed within dark matter halos, and not of the concentration of the dark matter of these halos. This point was emphasized by Nagai & Kravtsov (2005) in their investigation of a set of hydrodynamic simulations of clusters, in which they found values of $c_{\rm gal} \sim 2-7$ for eight clusters where the dark matter concentrations were $\sim 6-16$. In general, for any population of galaxies in a host halo, the radial distribution is dependent on the dynamical and star formation histories of the galaxies once they enter the host halo and may depend sensitively on how the population is selected (Diemand et al. 2004; Gao et al. 2004; Nagai & Kravtsov 2005). Mandelbaum et al. (2004) have found that low values of $c_{\rm gal}$ quite similar to what we measure here are required to match the galaxy-galaxy lensing observations in SDSS.

6. CLUSTER LUMINOSITY FUNCTIONS FOR $M_r < -18$ WITHIN $R_{200}^{\mathcal{N}}$

We can use $R_{200}^{\mathcal{N}}$ to compare commensurate regions within clusters of different richness. We first measure the LF per unit surface area of cluster members within the appropriate $R_{200}^{\mathcal{N}}$ for each richness, then rescale by the area contained within $R_{200}^{\mathcal{N}}$ to determine the actual number of galaxies of each brightness within $R_{200}^{\mathcal{N}}$ for each richness. We combine the LFs into six bins of $N_{\rm gal}$. The top panel of Figure 10 shows the LFs of all galaxies within $R_{200}^{\mathcal{N}}$; in the bottom panel those galaxies identified as BCGs have been removed.

With the BCGs removed, a Schechter function provides a reasonable fit to the data in all $N_{\rm gal}$ ranges. Blanton et al. (2004) have examined the LF of low-luminosity galaxies, finding that surface brightness selection effects bias the LF to lower values fainter than $M_r \sim -18$. That is, low-luminosity, low surface brightness galaxies tend to be missed. In addition, Blanton et al. (2004) find that the field galaxy LF turns up fainter than $M_r \sim -18$ and that the shape of the LF over a wide range of magnitudes is best fitted by a double Schechter function. In light of the concerns about missing low surface brightness galaxies at faint magnitudes, we restrict our fit to $M_r < -18$. For $N_{\rm gal} \geq 8$, $\alpha = -1$ provides a reasonable fit to the data in this magnitude range. The parameters of the Schechter function fits, with α fixed, are listed in Table 2. The two lowest richness bins are not well fitted with a faint-end slope of -1; in the table we list the best-fitting Schechter function parameters for these two bins. Detailed investigation of the differences in LF between different richness samples will be done in future work with a more extensive data set. However, we see that the primary change is the increase in normalization of the LF with increasing cluster richness, that the characteristic luminosity, M_*, brightens moderately toward richer clusters, and that the $N_{\rm gal} < 8$ systems are different from the richer objects. The mean redshift of the different richness cluster samples changes by $\Delta \ddot{z} \sim 0.03$, so we do not expect significant luminosity evolution ($\Delta M_* < 0.1$ mag). We note that since these LFs are determined using cluster members that reside

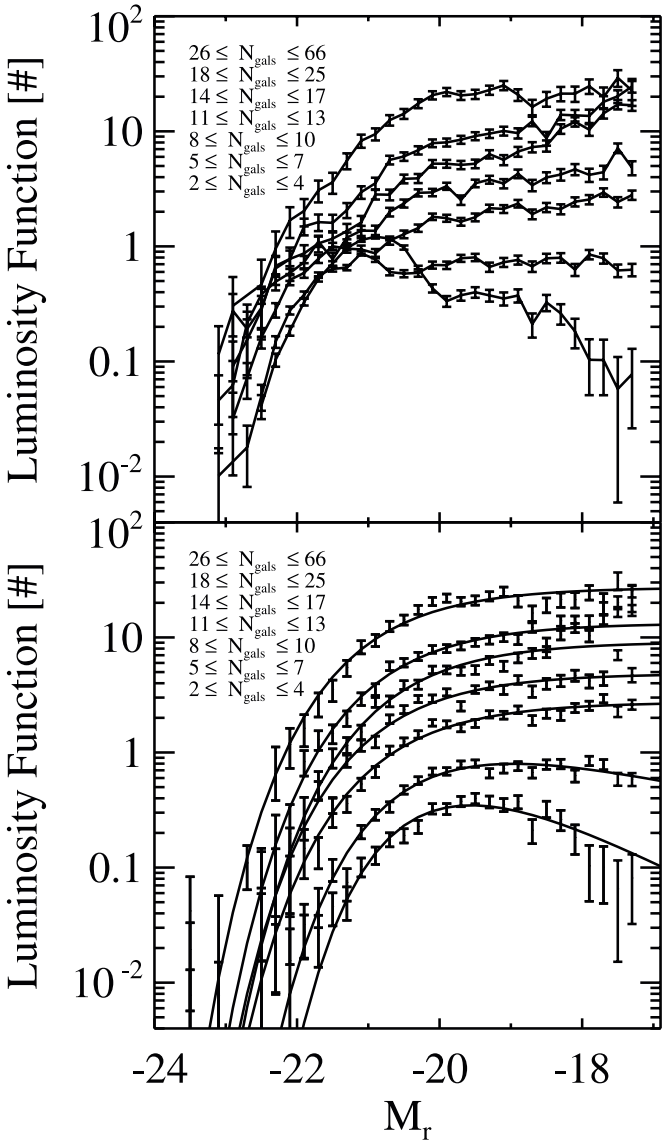

FIG. 10.—LF within $R_{200}^{\mathcal{N}}$, expressed as the number of galaxies per magnitude, for galaxies in clusters of different richnesses. *Top*: LFs of all galaxies within $R_{200}^{\mathcal{N}}$. A Schechter function is not a good fit to many of the richness bins, as the effect of the BCG is significant. *Bottom*: LFs for the same sets of clusters as above, but with those galaxies identified as BCGs removed. Schechter functions fitted for $M_r < -18$ are shown; the faint-end slope was held fixed for bins with $N_{\rm gal} \geq 8$. The parameters and χ^2 of the fits are listed in Table 2. [*See the electronic edition of the Journal for a color version of this figure.*]

TABLE 2
SCHECHTER FITS FOR r-BAND LUMINOSITY FUNCTIONS WITHIN $R_{200}^{\mathcal{N}}$, BCGS EXCLUDED

Richness	M_*	α	ϕ_*	χ^2/dof
$2 \leq N_{\rm gal} \leq 4$.....	-19.95 ± 0.12	-0.38 ± 0.12	0.94 ± 0.07	1.2
$5 \leq N_{\rm gal} \leq 7$.....	-20.06 ± 0.08	-0.55 ± 0.07	1.89 ± 0.12	1.2
$8 \leq N_{\rm gal} \leq 10$.....	-20.65 ± 0.04	-1.00 (fixed)	2.93 ± 0.09	1.8
$11 \leq N_{\rm gal} \leq 13$.....	-20.68 ± 0.04	-1.00 (fixed)	5.29 ± 0.17	2.3
$14 \leq N_{\rm gal} \leq 17$.....	-20.58 ± 0.05	-1.00 (fixed)	9.53 ± 0.33	2.0
$18 \leq N_{\rm gal} \leq 25$.....	-20.70 ± 0.04	-1.00 (fixed)	14.1 ± 0.47	1.1
$26 \leq N_{\rm gal} \leq 66$.....	-20.86 ± 0.05	-1.00 (fixed)	29.9 ± 1.07	1.9

within $R_{200}^{\mathcal{N}}$, the local density is the same on average for these galaxies, so the richness dependence of the LFs may not be attributed solely to variations in the local environment.

The sensitivity of the shape of the LF to the cluster richness makes comparison between different catalogs of clusters difficult. Different definitions of richness and/or different bins of richness will result in different measured LFs. In addition, other catalogs typically present results for the LF using galaxies within a fixed physical aperture, rather than within an aperture that scales with mass. Some authors rescale individual cluster LFs by cluster richness before creating a composite LF but still examine the LF within a fixed physical aperture. Nonetheless, we do find qualitatively similar results to other authors. The LF we find for rich clusters is similar to the LF of rich clusters presented in Goto et al. (2002b), who used the same SDSS data but a different cluster-finding algorithm and different method of background subtraction. Our results are also in agreement with those of Popesso et al. (2005). Like Popesso et al. (2005), we see that the faint end of the LF picks up below $M_r \sim -18$, even though we are likely missing some of these faint galaxies due to surface brightness selection effects. Our LFs in other bands are also comparable to the measurements of other authors, who typically find a steeper faint end in bluer bandpasses. Table 1 of Popesso et al. (2005) lists the Schechter parameters for composite cluster LFs retrieved from the literature for a variety of bandpasses. The LFs in lower richness bins are also comparable to what has been found by other authors. The $8 \leq N_{\rm gal} \leq 10$ groups are comparable to those of Martínez et al. (2002), with velocity dispersions $\sim$300 km s^{-1}; we find a similar result to theirs for the LF of these groups when we, like they, include the BCG. The LFs of very low richness systems ($N_{\rm gal} \leq 8$) have a falling faint-end slope and a bright end that is dominated by the BCGs of these objects. These are the same systems that are preferentially found in underdense regions, as shown in § 3.2.1. We discuss these systems further in § 7.

With the BCGs included, a Schechter function is not a good description of the data, except for in the very richest clusters where they are only a small contribution: the BCG population adds a bright-end "bump" to the LF of the other cluster members. The BCGs tend to be increasingly bright in higher mass clusters but also become less important to the total light with increasing cluster mass. We fit the LFs within $R_{200}^{\mathcal{N}}$, BCGs included, with a Gaussian for the BCGs plus a Schechter function for the non-BCG galaxies. This model is a good fit to the data for all $N_{\rm gal}$ ranges. The top panel of Figure 11 shows the relative amplitudes of the Schechter function and the Gaussian function, $f_{{\rm Sch},\mu}$, evaluated at the mean of the Gaussian component as a function of mean $\log N_{\rm gal}$. Over this range the trend is linear, with $f_{{\rm Sch},\mu} \sim N_{\rm gal}/38.3$. This scaling is the observed analog for the SDSS to the conditional baryonic mass function investigated by Zheng et al. (2004; see their Fig. 9).

We plot the mean luminosity of the Gaussian as a function of mean $\log N_{\rm gal}$ in the bottom panel of Figure 11. The trend of brighter BCGs in richer clusters is evident. Over the range we probe, our data are consistent with a single power law, $L_c \sim N_{\rm gal}^{0.5}$. This result is similar to, but slightly steeper than, the scaling with mass found by other authors (Lin & Mohr 2004; Zheng et al. 2004; van den Bosch et al. 2004), but note that we are plotting the scaling as a function of $N_{\rm gal}$ and not mass. Our data are all for multiple-galaxy systems and as such cannot constrain the very low mass end of the distribution studied by others. However, in order to facilitate comparison with previous work (Vale & Ostriker 2004; see also the compilation of Cooray & Milosavljević 2005), we fit a double power-law function with several parameters fixed to agree with the low-mass behavior of Vale & Ostriker (2004). We find that the relationship between mean BCG luminosity and $N_{\rm gal}$ is consistent with a model of the form

$$L_c/L_* = \frac{\left(N_{\rm gal}/N_c\right)^4}{\left[1 + \left(N_{\rm gal}/N_c\right)\right]^{\gamma}}, \qquad (6)$$

where the mean BCG luminosity, L_c, is scaled to L_* of the LF for SDSS galaxies (Blanton et al. 2003b). The best-fit parameters are $N_c = 0.98 \pm 0.04$ and $\gamma = 3.52 \pm 0.02$, but we stress that these are degenerate with the parameters we have held fixed; our current data cannot put a strong constraint on the exponent in the numerator (specifying the scaling for low masses). We note that the observation that BCGs are drawn from a different LF from other cluster members is well known (see, for example, the review by Collins et al. 2003 and references therein). The trend of increasing central galaxy luminosity with cluster richness has also been noted in many other observational studies, such as Sandage & Hardy (1973), Sandage (1976), Hoessel et al. (1980), Schneider et al. (1983), and Lin & Mohr (2004), and is consistent with predictions from the semianalytic models of Benson et al. (2003) and Zheng et al. (2004).

Local density is known to correlate with several galaxy properties, including luminosity (Blanton et al. 2003b), and so we also expect to see differences in the LF as a function of radius. Figure 12 shows the LF of galaxies in three radial bins: $0.0 \leq r/R_{200}^{\mathcal{N}} < 0.25$ (*thin lines*), $0.25 \leq r/R_{200}^{\mathcal{N}} < 0.75$ (*medium-weight lines*), and $0.75 \leq r/R_{200}^{\mathcal{N}} < 1.75$ (*thick lines*) for galaxies in clusters in four bins of richness. For the innermost radial

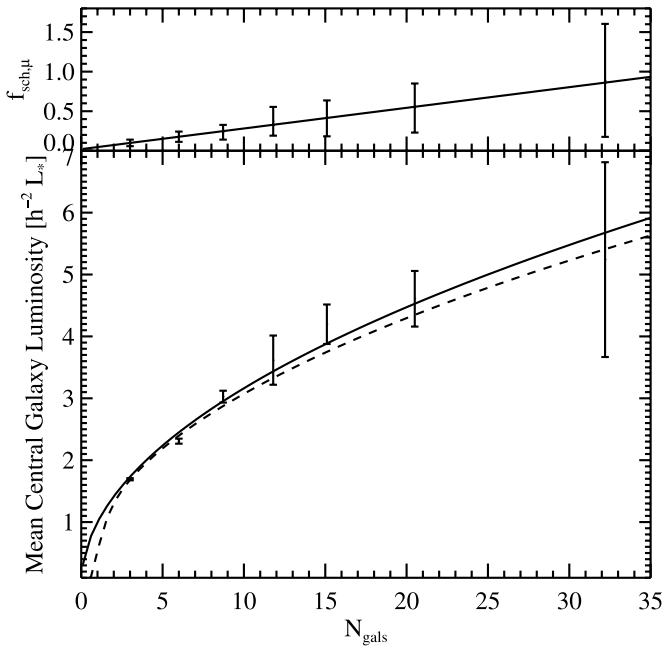

FIG. 11.—Parameters related to fitting the LFs within $R_{200}^{\mathcal{N}}$, BCGs included, with a model comprised of a Gaussian (for the BCGs) plus a Schechter function (for the non-BCGs), plotted as a function of the mean $\log N_{\rm gal}$ for the ranges used. The LFs used are the same as in the top panel of Fig. 10. *Top*: Ratio of the amplitudes of the Schechter and Gaussian functions evaluated at the mean μ of the Gaussian component. The best-fit line is plotted and has $f_{{\rm Sch},\mu} \sim N_{\rm gal}/38.3$. *Bottom*: Mean luminosity μ of the Gaussian fit to the LF of the BCGs, in terms of L_* for SDSS galaxies, as a function of cluster richness. The solid line is $L = N_{\rm gal}^{1/2}$; the dashed line is the double power-law model of eq. (6).

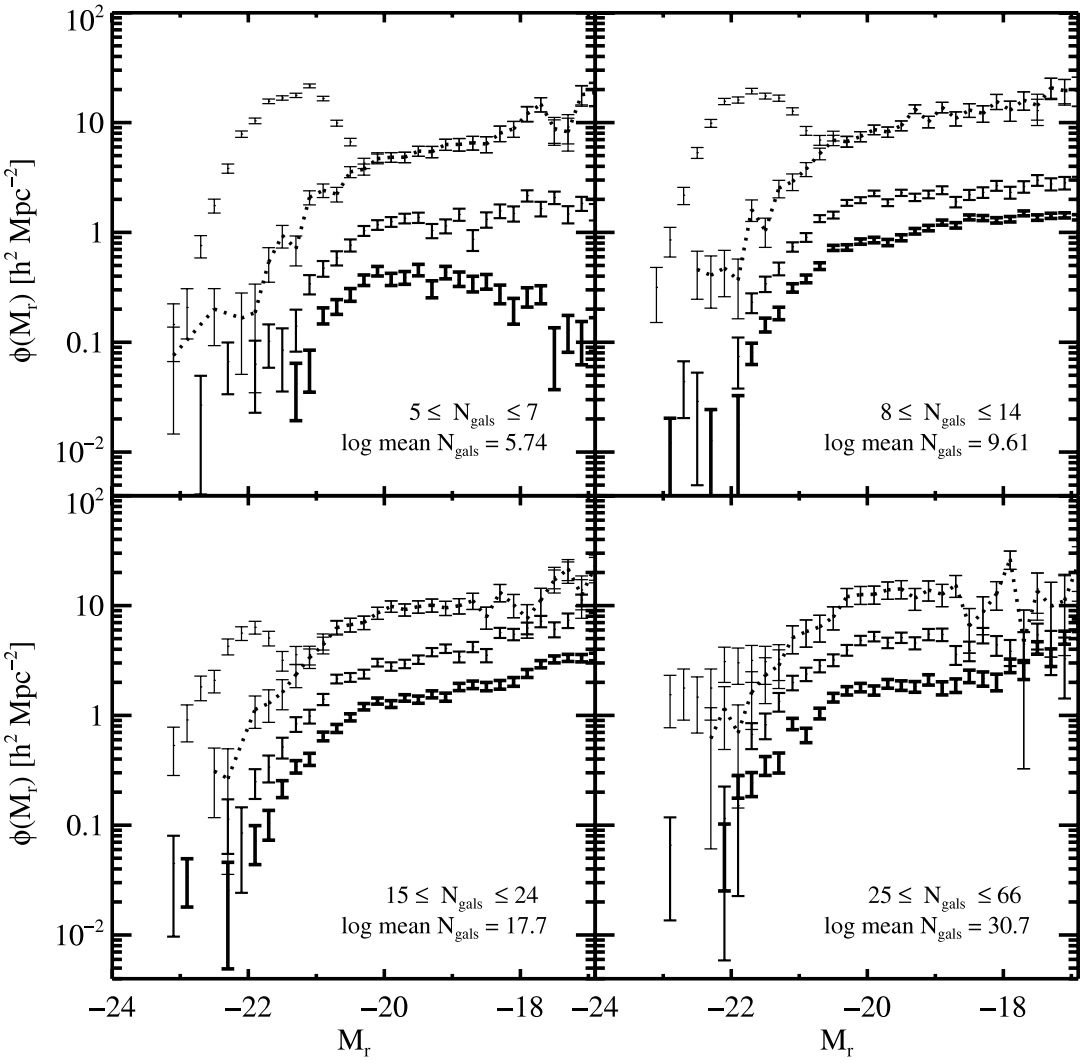

FIG. 12.—LF per unit surface area of galaxies in clusters of different richness as a function of distance from the cluster center in terms of $R_{200}^{\mathcal{N}}$. Thin lines are galaxies within $r/R_{200}^{\mathcal{N}} < 0.25$ (the dotted line indicates the LF with the BCGs removed); medium-weight lines are galaxies in the range $0.25 \leq r/R_{200}^{\mathcal{N}} < 0.75$; thick lines are galaxies in $0.75 \leq r/R_{200}^{\mathcal{N}} < 1.75$. For all richnesses, the overall normalization of the LF decreases toward larger radii, as the density of galaxies drops. Very bright galaxies are found predominantly only in the centers of both poor and rich objects. Note that the BCG population tends to be brighter and less dominant as cluster richness increases.

bin, we plot the LF both with and without (*dotted lines*) the BCGs. For these LFs, we plot the LF per unit surface area to explicitly show the change in local density. For all richnesses, the overall normalization of the LF decreases toward larger radii, as the density of galaxies drops. Very bright galaxies are found predominantly only in the centers of both poor and rich objects. Except for the lowest richness systems, the faint-end slope is roughly similar for all radial bins, although M_* shifts somewhat fainter toward the outskirts of the clusters. The data are not statistically powerful enough to put strong constraints on these variations; future work with a more extensive data set will allow more detailed investigation. We have not plotted the data for $N_{gal} < 5$ objects, as just beyond $R_{200}^{\mathcal{N}}$ of these objects the radial profile becomes negative, as these objects live in underdense regions. However, the LFs of these systems, both with and without BCGs, within $0.25r/R_{200}^{\mathcal{N}}$ are similar to the LF found for $5 \leq N_{gal} \leq 7$ groups, although with a slightly fainter centroid of the BCG population.

Our cluster-finding algorithm identifies the BCG as the galaxy that maximizes $\mathcal{L}(z)$, a statistic that incorporates luminosity, color, and the number of fainter neighbors of similar color. There is an interplay between maximum local density and finding a galaxy with the right luminosity and color to be a BCG. Sometimes the maximum total likelihood selects a galaxy as BCG that the eye would not. The cluster center is defined to be at the location of the algorithm-defined BCG and thus may not be at the true center of the cluster potential if the most massive cluster member is not the one with the highest BCG likelihood and/or is not at the center of the potential. Tests with simulations suggest that the centering of the maxBCG algorithm is good within $\sim 80\, h^{-1}$ kpc. For a rich cluster, this amount is a small fraction of the virial radius, but for a poor group, the algorithm may misplace the cluster center by one-third of the virial radius. Even if the galaxy identified as the BCG is both the brightest and the closest to the cluster center, X-ray observations suggest that a BCG can reside as far as $\sim 70\, h^{-1}$ kpc from the center of the X-ray emission (Lazzati & Chincarini 1998; Lin & Mohr 2004).

The inner region of the lowest richness objects may be biased due to failing to correctly identify the galaxy most closely located at the center of the cluster and therefore incorrectly positioning the center of the cluster. For the radial profiles, a higher inner radial bin due to incorrect removal of the BCG of the lower

richness objects will skew the measured concentration parameter to higher values for those objects. We also see the presence of BCG-like galaxies in the very inner regions of the lowest richness clusters in the LF: examining the region within 50 h^{-1} kpc of the centers of poor clusters shows an LF with a small "BCG bump" at the bright end, even when the maxBCG-identified BCGs are removed. Further investigation is needed to show whether these galaxies are the true BCGs of these groups, or whether the groups host a population of BCG-like galaxies in addition to the BCG.

7. DISCUSSION AND CONCLUSIONS

By using statistical background subtraction, we have observationally determined the changes in the radial distribution of cluster galaxies as a function of cluster richness and used that information to calculate a characteristic radius for clusters of each richness. This model-independent radius, $R_{200}^{\mathcal{N}}$, is based on the number density of galaxies analogously to the way R_{200} in use in simulations is based on mass density. We find that $R_{200}^{\mathcal{N}}$ exhibits a power-law scaling relationship with cluster richness. This result is in good agreement with the expected scaling from simulations.

Our result is also in general agreement with results obtained by other groups using different methods for measuring richness and R_{200}. Girardi et al. (1995) examined spectroscopically confirmed members of 90 rich clusters and determined virial and core radii by fitting the observed galaxy distribution with an isothermal sphere. They find virial radii of 0.5–1 h^{-1} Mpc, the same range we find for $R_{200}^{\mathcal{N}}$ for rich clusters. Yee & Ellingson (2003) examined R_{200} as a function of cluster richness $B_{\rm gc}$ (the amplitude of the galaxy cluster center correlation function measured for each cluster, scaled by an LF and spatial distribution) for 16 rich clusters with spectroscopically confirmed members. They measured R_{200} by applying a singular isothermal sphere model to the velocity dispersion data (Carlberg et al. 1997a) and find $R_{200} \sim B_{\rm gc}^{0.54\pm0.18}$. This scaling matches well with what we find, although with greater scatter than our result. With our techniques, we have been able to use photometric data to confirm this relationship for rich clusters and extend the relationship to much less rich systems.

To compare equivalent regions of clusters of different richness, $R_{200}^{\mathcal{N}}$ may be used as an aperture within which to compare the properties of cluster members. The space density distribution of galaxies within $R_{200}^{\mathcal{N}}$ is well described by an NFW profile, and the derived concentration parameter varies with cluster richness. We examined the population distribution function of cluster galaxies to determine how the LF of cluster members changes both radially and with cluster richness, using our determination of $R_{200}^{\mathcal{N}}$ to compare clusters in a wide range of richnesses. The radial variation of the LF of cluster galaxies is similar in clusters of all richnesses but does depend on the cluster richness. It is important to note that we can still detect a signal from the clusters at 2 h^{-1} Mpc from the cluster, even for poor groups. That there is still a significant overdensity at these distances suggests caution when measuring the contribution of the background in an annulus centered on the cluster.

We find that the central galaxies of clusters are distinguishable from the rest of the cluster galaxy population, as has been noted by others in both observational studies and theoretical models. The BCG population is clearly evidenced in the LF within $R_{200}^{\mathcal{N}}$ and more dramatically in the LF of the central region of clusters, as a "bump" at bright magnitudes that rises above the LF of the other cluster members. As the richness of the cluster increases, the BCG population becomes brighter but contributes less to the overall cluster light, in agreement with the results of K-band observations of BCGs in 93 X-ray–selected systems studied by Lin & Mohr (2004). We find that the LF of low- and intermediate-richness systems cannot be well described by a Schechter function when the BCGs are included; this function provides an acceptable fit only for the richer systems where the fractional contribution of the central galaxy to the LF is small. The total cluster LF within $R_{200}^{\mathcal{N}}$ is well modeled by the sum of a Gaussian for the central galaxy and a Schechter function for the satellites over the whole range of $N_{\rm gal}$. The trends of mean BCG luminosity and fractional contribution of the BCGs are in good agreement with the models of Zheng et al. (2004). We find that the mean BCG luminosity scales with mean $\log N_{\rm gal}$ as $N_{\rm gal}^{1/2}$, a similar yet slightly steeper result to what is seen in other studies.

The low-richness objects identified with our cluster-finding algorithm have properties that are quite different from rich clusters. Systems with $N_{\rm gal} < 5$ and $N_{\rm gal} > 7$ have clearly different radial profiles and LFs. The transition region $5 \leq N_{\rm gal} \leq 7$ has intermediate properties. One possible contribution to this difference is that the lowest $N_{\rm gal}$ objects are also the most likely to suffer from the effects of misidentifying the cluster center and/or the brightest cluster member. In addition, the $N_{\rm gal} < 8$ objects have a strong selection function: maxBCG is finding systems where specifically only a few red galaxies are within 1 h^{-1} Mpc of the galaxy identified as the BCG. It is interesting that demanding so few galaxies of that color be in the neighborhood has the effect of finding objects that have very concentrated radial profiles, are located in isolated regions, and are dominated by bright galaxies.

A possible explanation for these very low $N_{\rm gal}$ systems is that at least some of them are fossil groups. Observationally, a fossil group has the X-ray luminosity of a group or poor cluster, but in the optical, only a highly luminous early-type galaxy without bright neighbors is observed. The first such object was detected by Ponman et al. (1994); subsequent study has shown that there are a few other galaxies in this group, but all are significantly fainter ($\Delta m \geq 2.5$ mag) than the first-ranked galaxy (Jones et al. 2000). Other fossil groups have been identified as well (Mulchaey & Zabludoff 1999; Vikhlinin et al. 1999; Romer et al. 2000; Matsushita 2001). Such systems are thought to be the end product of groups in which most of the galaxies have merged, producing a highly luminous central galaxy mostly alone in a halo of hot X-ray gas. This scenario is supported by the observations that the central galaxies emit a very high fraction of the total optical light of the group and that there is a dearth of L_* galaxies in the central region of these systems (Jones et al. 2003).

At fixed halo mass, there is a theoretical expectation that there should be a correlation between halo formation time and the total number of galaxies above a given luminosity threshold (Zentner et al. 2005). This correlation may select a special population of clusters at low $N_{\rm gal}$. We speculate that in high-mass halos, all systems have bright red galaxies regardless of their formation time and are equally well found by the maxBCG algorithm, while in smaller, group-mass halos the requirement to select red galaxies may select only the earliest forming halos. These low-$N_{\rm gal}$ systems would be expected to be early-forming halos with higher than average masses for their $N_{\rm gal}$, whose outer satellites have already merged with the central object. This theory is consistent with the LF shape and the extremely steep radial profiles seen here, as well as with the higher masses that are indicated by cluster-mass correlation function examined by E. S. Sheldon et al. (2005, in preparation).

Many of these systems may also be classified as compact groups (CGs), such as those studied by Hickson (1982, 1993)

and others. CGs have been identified in SDSS data by Lee et al. (2004). They investigate the local environment of CGs and find that while on average the number density of surrounding galaxies is comparable to the local environment around field galaxies, there is considerable scatter to both more and less dense environments (see their Fig. 9). By demanding few other bright, red galaxies nearby, the maxBCG algorithm may be preferentially selecting fossil groups, which would also look like those CGs in environments with a low number density of neighbors. Further study is needed to understand this interesting set of systems. More investigation can be done using SDSS data, but it also would be interesting to look for an X-ray signal from a stacked set of these low-richness objects.

We draw attention to the range of LFs for galaxies within $R_{200}^{\mathcal{N}}$ of clusters of different richness and also to the differences in the LF seen radially. Such variation makes it difficult to compare between different cluster catalogs, where different proxies for mass and aperture are in use. The LFs of clusters in a mass range are different when different fractions of $R_{200}^{\mathcal{N}}$ are sampled, and different again when a fixed aperture is used for each cluster. Nonetheless, we do see similar results to those of other authors, including an upturn at the faint end for rich clusters. This effect comes primarily from galaxies located in the outer regions of the clusters.

We are currently working to compare our results with simulations to show how our space density–based $R_{200}^{\mathcal{N}}$ relates to the mass density–based R_{200} commonly used in N-body models. Also, we examine how our richness parameter, $N_{\rm gal}$, relates to mass M_{200} from the simulations. Further work will be done to use the rich SDSS data set to explore the distribution of many properties of cluster galaxies in addition to those considered here.

Using a small subset of the SDSS data is sufficient to determine the scaling of $R_{200}^{\mathcal{N}}$ with cluster richness and to robustly measure the LFs and radial profiles in small $N_{\rm gal}$ bins. Using the full SDSS data set will allow us to study $\sim$500 of the richest clusters and over 25,000 groups and will allow cluster detection to higher redshifts. We will check for evolution in our scaling relationship by examining the $R_{200}^{\mathcal{N}}$-$N_{\rm gal}$ trend in different redshift samples. Preliminary results indicate that the scaling is the same, but with higher normalization for lower redshift objects. To compare the properties of any stacked set of clusters, the relationship of $R_{200}^{\mathcal{N}}$ to $N_{\rm gal}$ is essential. We can now compare different mass estimates, including those measured from total luminosity, velocity dispersion, and lensing information. We will also use lensing studies to compare the profiles of the luminous and dark components of the clusters, more closely investigate the possible differences in concentration of the two profiles, and examine the bias between luminous and dark matter in these dense environments. Extending this work to include color and morphology indicators, we will probe many characteristics of galaxies in clusters, exploring the history of galaxy formation as a function of environment and studying the BCG population.

For large surveys it is typically not practical to determine cluster mass or size using spectroscopy. Without assuming a model for the distribution of galaxies, we provide a way to determine cluster size from photometric data alone for $z \leq 0.3$. With knowledge of how the size-mass scaling evolves and a better understanding of the scaling of $R_{200}^{\mathcal{N}}$ with total mass, our method provides a feasible way to measure the characteristic radii and masses of clusters that will be found in future large, high-redshift surveys.

Funding for the creation and distribution of the SDSS Archive has been provided by the Alfred P. Sloan Foundation, the Participating Institutions, the National Aeronautics and Space Administration, the National Science Foundation, the US Department of Energy, the Japanese Monbukagakusho, and the Max Planck Society. The SDSS Web site is http://www.sdss.org.

The SDSS is managed by the Astrophysical Research Consortium (ARC) for the Participating Institutions. The Participating Institutions are the University of Chicago, Fermilab, the Institute for Advanced Study, the Japan Participation Group, Johns Hopkins University, the Korean Scientist Group, Los Alamos National Laboratory, the Max-Planck-Institute for Astronomy (MPIA), the Max-Planck-Institute for Astrophysics (MPA), New Mexico State University, University of Pittsburgh, University of Portsmouth, Princeton University, the United States Naval Observatory, and the University of Washington.

S. M. H. was supported by a General Electric Faculty for the Future Fellowship and by the Michigan Space Grant Consortium. T. A. M. acknowledges support from PECASE grant AST 97-08232 and NSF grant AST 02-06277. R. H. W. was supported by NASA through Hubble Fellowship HF-01168.01-A awarded by Space Telescope Science Institute. We thank Gus Evrard, Andrey Kravtsov, Martin White, and Andrew Zentner for helpful discussions and suggestions.

REFERENCES

Abell, G. O. 1958, ApJS, 3, 211
Abell, G. O., Corwin, H. G., & Olowin, R. P. 1989, ApJS, 70, 1
Andreon, S., Willis, J., Quintana, H., Valtchanov, I., Pierre, M., & Pacaud, F. 2004, MNRAS, 353, 353
Aragon-Salamanca, A., Baugh, C. M., & Kauffmann, G. 1998, MNRAS, 297, 427
Bahcall, N. A. 1981, ApJ, 247, 787
Bahcall, N. A., et al. 2003a, ApJ, 585, 182
———. 2003b, ApJS, 148, 243
Bartelmann, M. 1996, A&A, 313, 697
Benson, A. J., Frenk, C. S., Baugh, C. M., Cole, S., & Lacey, C. G. 2003, MNRAS, 343, 679
Blanton, M. R., Lupton, R. H., Schlegel, D. J., Strauss, M. A., Brinkmann, J., Fukugita, M., & Loveday, J. 2004, ApJ, submitted (astro-ph/0410164)
Blanton, M. R., et al. 2001, AJ, 121, 2358
———. 2003a, AJ, 125, 2348
———. 2003b, ApJ, 592, 819
Bower, R. G., Lucey, J. R., & Ellis, R. S. 1992, MNRAS, 254, 601
Bullock, J. S., Kolatt, T. S., Sigad, Y., Somerville, R. S., Kravtsov, A. V., Klypin, A. A., Primack, J. R., & Dekel, A. 2001, MNRAS, 321, 559
Carlberg, R. G., Yee, H. K. C., & Ellingson, E. 1997a, ApJ, 478, 462
Carlberg, R. G., et al. 1997b, ApJ, 485, L13
Colless, M. 1989, MNRAS, 237, 799
Collins, C. A., & Mann, R. G. 1998, MNRAS, 297, 128
Collins, Ch., Brough, S., Burke, D., Mann, R., & Lynam, P. 2003, Ap&SS, 285, 51
Cooray, A., & Milosavljević, M. 2005, ApJ, 627, L89
Couch, W. J., Ellis, R. S., MacLaren, I., & Malin, D. F. 1991, MNRAS, 249, 606
Dalton, G. B., Efstathiou, G., Maddox, S. J., & Sutherland, W. J. 1992, ApJ, 390, L1
Davis, M., Efstathiou, G., Frenk, C. S., & White, S. D. M. 1985, ApJ, 292, 371
Diaferio, A., Kauffmann, G., Balogh, M. L., White, S. D. M., Schade, D., & Ellingson, E. 2001, MNRAS, 323, 999
Diemand, J., Moore, B., & Stadel, J. 2004, MNRAS, 352, 535
Eke, V. R., Cole, S., & Frenk, C. S. 1996, MNRAS, 282, 263
Evrard, A. E., et al. 2002, ApJ, 573, 7
Gal, R. R., de Carvalho, R. R., Lopes, P. A. A., Djorgovski, S. G., Brunner, R. J., Mahabal, A., & Odewahn, S. C. 2003, AJ, 125, 2064
Gao, L., White, S. D. M., Jenkins, A., Stoehr, F., & Springel, V. 2004, MNRAS, 355, 819
Garilli, B., Maccagni, D., & Andreon, S. 1999, A&A, 342, 408

Girardi, M., Biviano, A., Giuricin, G., Mardirossian, F., & Mezzetti, M. 1995, ApJ, 438, 527
Gladders, M. 2002, Ph.D. thesis, Univ. Toronto
Gladders, M. D., & Yee, H. K. C. 2000, AJ, 120, 2148
———. 2005, ApJS, 157, 1
Goto, T., et al. 2002a, AJ, 123, 1807
———. 2002b, PASJ, 54, 515
Hickson, P. 1982, ApJ, 255, 382
———. 1993, Astrophys. Lett. Commun., 29, 1
Hoessel, J. G., Gunn, J. E., & Thuan, T. X. 1980, ApJ, 241, 486
Hogg, D. W., Finkbeiner, D. P., Schlegel, D. J., & Gunn, J. E. 2001, AJ, 122, 2129
Jenkins, A., Frenk, C. S., White, S. D. M., Colberg, J. M., Cole, S., Evrard, A. E., Couchman, H. M. P., & Yoshida, N. 2001, MNRAS, 321, 372
Jones, L. R., Ponman, T. J., & Forbes, D. A. 2000, MNRAS, 312, 139
Jones, L. R., Ponman, T. J., Horton, A., Babul, A., Ebeling, H., & Burke, D. J. 2003, MNRAS, 343, 627
Katgert, P., Biviano, A., & Mazure, A. 2004, ApJ, 600, 657
Kochanek, C. S., White, M., Huchra, J., Macri, L., Jarrett, T. H., Schneider, S. E., & Mader, J. 2003, ApJ, 585, 161
Kravtsov, A. V., Berlind, A. A., Wechsler, R. H., Klypin, A. A., Gottlöber, S., Allgood, B., & Primack, J. R. 2004, ApJ, 609, 35
Lazzati, D., & Chincarini, G. 1998, A&A, 339, 52
Lee, B. C., et al. 2004, AJ, 127, 1811
Lidman, C. E., & Peterson, B. A. 1996, AJ, 112, 2454
Lima, M., & Hu, W. 2005, Phys. Rev. D, submitted (astro-ph/0503363)
Lin, Y., & Mohr, J. J. 2004, ApJ, 617, 879
Lin, Y., Mohr, J. J., & Stanford, S. A. 2004, ApJ, 610, 745
Lugger, P. M. 1986, ApJ, 303, 535
Lumsden, S. L., Nichol, R. C., Collins, C. A., & Guzzo, L. 1992, MNRAS, 258, 1
Lupton, R. H., Gunn, J. E., Ivezić, Z., Knapp, G. R., Kent, S., & Yasuda, N. 2001, in ASP Conf. Ser. 238, Astronomical Data Analysis Software and Systems X, ed. F. R. Harnden, Jr., F. A. Primini, & H. E. Payne (San Francisco: ASP), 269
Mahdavi, A., & Geller, M. J. 2004, ApJ, 607, 202
Mandelbaum, R., Tasitsiomi, A., Seljak, U., Kravtsov, A. V., & Wechsler, R. H. 2004, MNRAS, submitted (astro-ph/0410711)
Martínez, H. J., Zandivarez, A., Merchán, M. E., & Domínguez, M. J. L. 2002, MNRAS, 337, 1441
Matsushita, K. 2001, ApJ, 547, 693
Mulchaey, J. S., & Zabludoff, A. I. 1999, ApJ, 514, 133
Nagai, D., & Kravtsov, A. V. 2005, ApJ, 618, 557
Navarro, J. F., Frenk, C. S., & White, S. D. M. 1997, ApJ, 490, 493
Nelson, A. E., Gonzalez, A. H., Zaritsky, D., & Dalcanton, J. J. 2002, ApJ, 566, 103
Oemler, A. 1976, ApJ, 209, 693
Olsen, L. F., et al. 1999, A&A, 345, 681
Ostrander, E. J., Nichol, R. C., Ratnatunga, K. U., & Griffiths, R. E. 1998, AJ, 116, 2644
Paolillo, M., Andreon, S., Longo, G., Puddu, E., Gal, R. R., Scaramella, R., Djorgovski, S. G., & de Carvalho, R. 2001, A&A, 367, 59
Peacock, J. A. 1999, Cosmological Physics (Cambridge: Cambrige Univ. Press)
Peebles, P. J. E. 1993, Principles of Physical Cosmology (Princeton: Princeton Univ. Press)
Petrosian, V. 1976, ApJ, 209, L1
Ponman, T. J., Allan, D. J., Jones, L. R., Merrifield, M., McHardy, I. M., Lehto, H. J., & Luppino, G. A. 1994, Nature, 369, 462
Popesso, P., Boehringer, H., & Voges, W. 2005, A&A, 433, 415
Postman, M., & Lauer, T. R. 1995, ApJ, 440, 28
Postman, M., Lauer, T. R., Oegerle, W., & Donahue, M. 2002, ApJ, 579, 93
Postman, M., Lubin, L. M., Gunn, J. E., Oke, J. B., Hoessel, J. G., Schneider, D. P., & Christensen, J. A. 1996, AJ, 111, 615
Romer, A. K., et al. 2000, ApJS, 126, 209
Sandage, A. 1972, ApJ, 178, 1
———. 1976, ApJ, 205, 6
Sandage, A., & Hardy, E. 1973, ApJ, 183, 743
Schechter, P. 1976, ApJ, 203, 297
Schlegel, D. J., Finkbeiner, D. P., & Davis, M. 1998, ApJ, 500, 525
Schneider, D. P., Gunn, J. E., & Hoessel, J. G. 1983, ApJ, 264, 337
Scranton, R., et al. 2002, ApJ, 579, 48
Sheldon, E. S., et al. 2001, ApJ, 554, 881
———. 2004, AJ, 127, 2544
Smail, I., Edge, A. C., Ellis, R. S., & Blandford, R. D. 1998, MNRAS, 293, 124
Smith, J. A., et al. 2002, AJ, 123, 2121
Stanford, S. A., Eisenhardt, P. R. M., & Dickinson, M. 1995, ApJ, 450, 512
Stoughton, C., et al. 2002, AJ, 123, 485
Vale, A., & Ostriker, J. P. 2004, MNRAS, 353, 189
Valotto, C. A., Nicotra, M. A., Muriel, H., & Lambas, D. G. 1997, ApJ, 479, 90
van den Bosch, F., Yang, X., & Mo, H. J. 2004, in Baryons in Dark Matter Halos, ed. R. Dettmar, U. Klein, & P. Salucci (Trieste: SISSA), 41
van der Marel, R. P., Magorrian, J., Carlberg, R. G., Yee, H. K. C., & Ellingson, E. 2000, AJ, 119, 2038
Vikhlinin, A., McNamara, B. R., Hornstrup, A., Quintana, H., Forman, W., Jones, C., & Way, M. 1999, ApJ, 520, L1
Weinberg, D. H., Davé, R., Katz, N., & Hernquist, L. 2004, ApJ, 601, 1
White, M. 2001, A&A, 367, 27
Yee, H. K. C., & Ellingson, E. 2003, ApJ, 585, 215
Yee, H. K. C., & López-Cruz, O. 1999, AJ, 117, 1985
York, D. G., et al. 2000, AJ, 120, 1579
Zehavi, I., et al. 2004, ApJ, 608, 16
Zentner, A. R., Berlind, A. A., Bullock, J. S., Kravstov, A. V., & Wechsler, R. H. 2005, ApJ, 624, 505
Zheng, Z., et al. 2004, ApJ, submitted (astro-ph/0408564)